Anonymous Referee #1
Received and published: 2 November 2020

The manuscript submitted by Evangeliou et al. investigates how COVID-19 related lockdowns impacted the levels of BC in Europe. They found a decline in BC emissions with a regionality showing strong links between the magnitude of emission decline and the severity of restrictions. The paper is well written and based on sound analyses. Authors include an account of sources of uncertainty in the presented results, and further support their findings by data from other sources. Papers investigating the effects on the current pandemic on climate and emissions are important contributions to the field, and I recommend the paper to be published after relatively minor revisions.

General comment: Authors use a well-developed scientific language. However, a reader not familiar with these method may at times be confused. Some very small adjustments may improve this. My comments exclusively pertain to the first part of the manuscript.

Response: We appreciate reviewer's willingness to help us improve this manuscript. We have tried to follow all of his comments.

Specific comments:

L 48: "Despite the socioeconomic impacts". The sentence is entirely correct, but it too easily reads as if the air quality has improved despite the societal impacts (which have lead to reduced emissions, which is the cause of the air quality improvement). I had to read it a couple of times to get its correct meaning. Since everything else is so fluent and well written here, I suggest to improve this sentence. A suggestion could be to start it as "In contrast to the detrimental societal impacts" or something similar.

Response: We have corrected the sentence as reviewer pointed (L48-50): "In contrast to … pollutant emissions".

L 55: "in at the beginning of" –> delete either "in" or "at"

I enjoyed reading this introduction, it really sets the research into context and is a great motivation for the importance of the results to come. Well done.

Response: We removed "at" (L 56). We kindly thank the reviewer for reading and altering on our manuscript.

L 245: Maybe this is just me, but "the aforementioned numbers" makes me look further up than to the last sentence. If you refer to the numbers 191/239 kt in this study/Eclipsev6, could you simply say "these numbers"?

Response: We replaced "aforementioned" with "these" (circa L 303, p 11) as suggested by the reviewer.

L 274: I am very tempted to think that the fact that the posterior emissions are lower than the prior ECLIPSEv6 emissions is solely due to COVID-19, which shows that I have not entirely understood your methods. You have a nice sentence on line 284 explaining that this is not so, but if you could move/repeat this, in more words, to some- where around line 274, this would help prevent misunderstandings. Could you write out clearly, here or in the methods section, what a smaller posterior emission number that the prior emission input could potentially mean and why?

Response: The inversion algorithm itself tries to better match modelled concentrations with observation by correcting emissions (of course taking into account some uncertainties). Since we calculated decreased posterior emissions throughout the whole inversion period (before and during the lockdowns), we cannot conclude that this is due to COVID-19 restrictions. To confirm COVID-19 impact on the emissions, we first need to compare with what was happening with emissions in previous years, as well as with emissions before and during the lockdown measures. We have now tried to clarify this in the text (circa L 350-357, p 11).

L 278: Again, it is not entirely clear to me what "posterior decreases" mean here – do you simply point to the fact that posterior emissions are lower than the prior emissions, or is there some time aspect that I am missing here, so that the decrease refers to something else? Please clarify in the text. Perhaps consider sticking to the word "difference" instead of "decrease" here?

Response: Yes, the expression refers to prior – posterior differences. We have now corrected it as suggested (circa L 304, p11).

L 281: While you state further up that the largest posterior decrease is in Eastern Europe, with a drop from 35 to 29 kt, Southern Europe had a decrease from 61 to 48 kt, which is higher? It would be good to look over this section and clarify this – perhaps also a more consistent way of reporting differences in percentual and/or absolute numbers would help?

Response: The answer here already exists in the text (L 334: "these numbers refer to the whole inversion domain (not only Europe) and …"), but we agree with the reviewer that can be clarified further. We have now included the exact definitions of the areas mentioned in the text (circa L 336-346, p11).

L 283: Please fix sentence (the last "were slightly enhanced" can be deleted).

Response: We have corrected this in p 11 (circa L 295). "were slightly enhanced" was deleted.

L 285: consider "the decrease" –> "the general decrease in emissions" to make clearer that this last sentence is about the overall decrease found (as it contrasts the previous sentence on Poland and Spain).

Response: The whole explanation there has been changed in a way to tackle reviewer's previous comment and explain in a more comprehensive way why a change in posterior emissions does not necessarily imply a COVID-19 impact.

Anonymous Referee #2
Received and published: 4 December 2020

In this work the changes in black carbon emissions (BC) due to the restrictions imposed in response to the global pandemic are estimated through inverse modeling. Absorp- tion measurements from the Aerosol, Clouds and Trace Gases Research Infrastructure (ACTRIS) and the networks European Monitoring and Evaluation Program (EMEP) are used in a Bayesian inversion system to estimate weekly emissions over Europe for a given a priori emission inventory. Estimated posterior BC emissions are compared against dependent observations first to examine the optimal prior inventory to con- duct the study. Then, concentrations computed with the estimated emissions were compared against two ARCTIS stations not considered in the inversion and therefore representing independent observations. Additionally, comparison was also conducted against reanalysis dataset of BC from MERRA-2 (Modern-Era Retrospective Analysis for Research and Applications Version 2). The results of this study suggest that BC emissions during the lockdown period were 10% smaller than for the same period of the previous five years. In addition, emissions decreased 10% over Europe when compared to the period before the lockdown. Although the study and the results are interesting, I find the article not well written. Before I can recommend it for publication it needs to be improved in terms of clarity and analysis. In what follows I'll present the general comments supporting my evaluation.

Response: We appreciate reviewer's effort to improve the manuscript.

General comments

1. Section 2 (Methods) is a description of different pieces used in the study without explaining the links between them and how they contribute to achieve the goal. The methodology was made clear while reading the Results. This should not happen; the full methodology should be clear to the reader while reading section 2. I suggest that an introductory paragraph should be included at the beginning of section 2 explaining the general methodology applied in the study and pointing to the individual sections where more information is provided. I believe it would also contribute if the inversion system is presented after all other elements used in the system have been presented.

Response: As suggested by the reviewer, we have added a full paragraph in the beginning of Methods section that describes in detail how each methodology and dataset used in the present is connected in conducting the assessment of the COVID-19 impact on BC emissions over Europe (L 109-126, p 5).

2. The authors provide an incomplete description of the inversion system. It is not clear from the text what the size of the state vector is? Are the emissions estimated for each grid illustrated in Figure 1 or are these grids aggregated to larger regions? Furthermore, how are the B and R matrices defined? Are the uncertainties of the prior considered not to be spatially correlated and thus the B matrix defined as a diagonal matrix? What about the R matrix is it also considered to be a diagonal matrix? The au- thors describe how they validate the chosen values but do not present the values used in either matrix. This is relevant information that should be provided by the authors. If it is provided in another study it should nevertheless be summarized in the paper.

Response: The Bayesian inversion algorithm that was used in the present study has been previously used in several applications (see references therein). We thought that giving all the details of the method would be a repetition, since we give the main references that describe it (Thompson and Stohl,2014; Thompson et al., 2015; Stohl et al., 2010). However, as pointed by the reviewer, we were obviously mistaken and, therefore, have amended this part and now give detailed information on the several definitions used in section 2.3 (Track changes circa L 175 and below).

Stohl, A., Kim, J., Li, S., O'Doherty, S., Salameh, P. K., Saito, T., Vollmer, M. K., Wan, D., Yao, B., Yokouchi, Y. and Zhou, L. X.: Hydrochlorofluorocarbon and hydrofluorocarbon emissions in East Asia determined by inverse modeling, Atmos. Chem. Phys. Discuss., 10(2), 2089–2129, doi:10.5194/acpd-10-2089-2010, 2010.

Thompson, R. L. and Stohl, A.: FLEXINVERT: An atmospheric Bayesian inversion framework for determining surface fluxes of trace species using an optimized grid, Geosci. Model Dev., 7(5), 2223–2242, doi:10.5194/gmd-7-2223-2014, 2014.

Thompson, R. L., Stohl, A., Zhou, L. X., Dlugokencky, E., Fukuyama, Y., Tohjima, Y., Kim, S. Y., Lee, H., Nisbet, E. G., Fisher, R. E., Lowry, D., Weiss, R. F., Prinn, R. G., O'Doherty, S., Young, D. and White, J. W. C.: Methane emissions in East Asia for 2000-2011 estimated using an atmospheric Bayesian inversion, J. Geophys. Res. Atmos., 120(9), 4352–4369, doi:10.1002/2014JD022394, 2015

3. The authors use 6 emission inventories as prior for the inversion and from those one (ECLIPSE v6) is chosen to conduct the study. Most, if not all, of these inventories do not provide yearly estimates but for larger intervals. ECLIPSE for instance provides estimates every 5 years. How do the authors deal with this? Do they linearly interpolate between the available years to have yearly estimates? Furthermore, while 2015 in ECLIPSE correspond to an actual estimate, the emission for 2020 correspond to a projection. None of the priors for 2020 are an actual estimate but a projection of some kind. Do the authors attribute larger uncertainties to the prior of 2020 because of this? In other words is the B matrix defined differently for 2020? If not, why? What is the impact on the results due to this difference between emissions before 2020 and the projected emissions for 2020?

Response: As we demonstrate in the following figure, the anthropogenic emissions of BC in Europe between January-April 2015 and January-April 2020 differ by 3.4% only, and, therefore, we do not interpolate emissions in the years from 2015 to 2020. What we do is that we only add biomass burning emissions from GFED4 every year, as those have a spatiotemporal impact to the total emissions of BC.

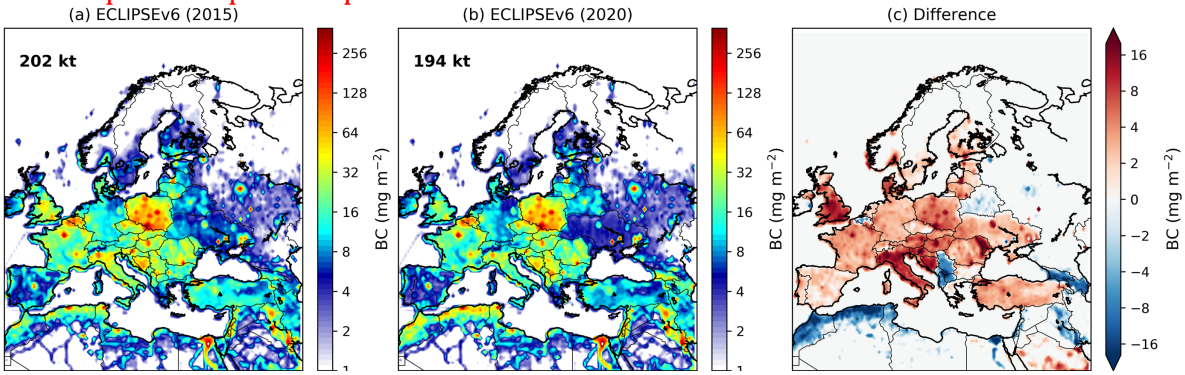

As regards to the uncertainty of the prior emissions, we do not consider inversions as a black box to give random uncertainty to the prior source, and we rather treat the errors very carefully. For example, inappropriate chosen prior uncertainties can cause spurious negative emissions. Especially if prior uncertainties are too large, there may be a

problem of over-fitting the observations, where the observation uncertainty is smaller than the model representation error, such that the model cannot even with the "true" emissions possibly fit the observations within the uncertainty range. To choose realistic uncertainties, we use reduced chi-square value (the value of the cost function at minimum divided by number of observations and divided by 2) which should be around 1. The probability density function (pdf) of prior and posterior model-observation differences (i.e. BC concentrations) is compared with the pdf where 1SD is given by the measurement error. If all values have been well chosen, the posterior model-observation differences should fit (very) approximately the pdf

4. Different set of stations were used for the period 2015-2019 and 2020. As the authors state in sections 3.3, changing observations can have drastic impact on the posterior emissions. Why were different stations used for the two periods? How many stations would be available for the inversion if only stations with data for both periods were used? How do the results change if only these stations are used in the inversion? The authors should discuss how the fact of using different set of stations impact the results. Ideally, the authors should demonstrate that the results are not impacted by using different set of observations between both periods.

Response: Unfortunately, it was not possible to have measurements from the same stations every year for different reasons (e.g. instrument failures and other deficiencies or simple late or no reporting of measurements). As explained in the Methods section, the different station measurements result in different average source-receptor matrices (SRMs) and, in turn, in different aggregated grid. To minimize the impact of using slightly different station measurements (due to different data availability), we used exactly the same grid for all inversions, as otherwise differences in the posterior emissions can partly be due to different grid geometries.
Since it is not possible to use exactly the same stations for the 2015-2019 inversions as for the 2020 (due to different station data availability), we prove that the difference in the posterior is rather small when using slightly different station data. For this, we performed an inversion using the stations of our main inversion in 2020 (Table 1) and another after removing 4 stations in Spain and Italy (ES0018G, ES0020U, ES0022R and IT0004R, see Table 1). In this way, we used 17 stations in our standard inversion set-up and 13 (17-4) stations. This fraction of different stations is similar to this of the 2015-2019 set-up versus the 2020 inversion set-up:

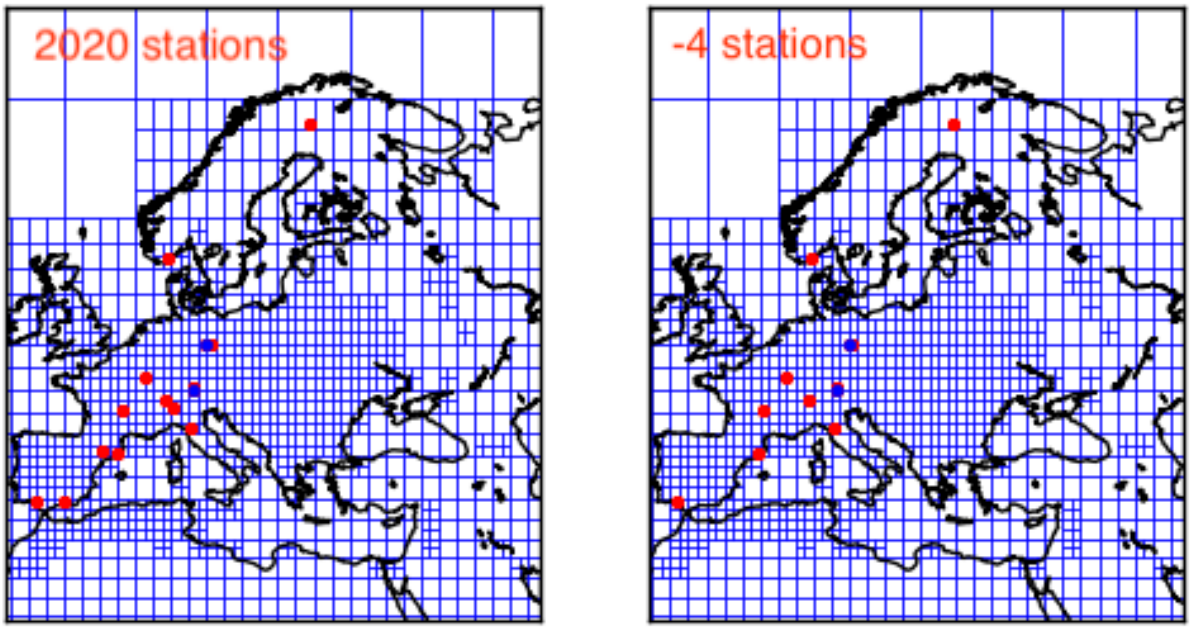

We found that the difference in posterior emissions of BC is tiny and does not affect the final result more than 1% (191 kt versus 189 kt).

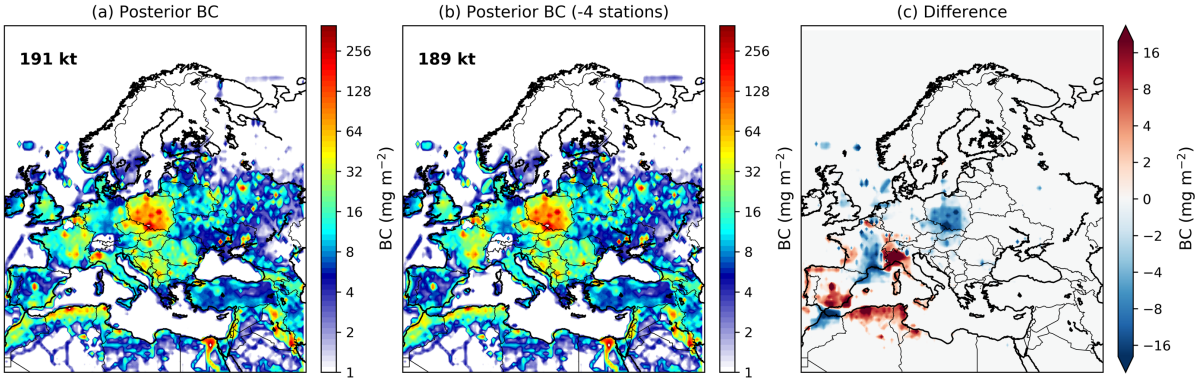

Specific comments

Lines 50-52: The two periods considered in the analysis should be included.

Response: We do not understand what periods the reviewer means here. One period is considered (January to March 2020). We just give an indication about what happened in the previous 5 years using the same methodology (inverse modelling combined relevant measurements). If the reviewer insists in this change with a more precise comment, we will change this in a next step.

Lines 59-62: The formulation of this sentence can be improved. The sentence is started with "Except" and then continued with "also". What is the point of using "Ex- cept"?

Response: We have now tried to improve this sentence. All we tried to do here with the use of "except" was to link the apparent decrease in the 2020 emissions compared with previous years' emissions with the decrease of the emissions when the period before and during lockdown was compared.

Line 74: Is "distancing" missing after "strict social".

Response: No, there is nothing missing here: "… strict social, travel and working restrictions …". "Strict social" is linked to "restrictions".

Line 120: Acronym MAC needs to be defined.

Response: Thanks to the reviewer, the acronym is now explained where it appears first in the text (see Track Changes).

Lines 148-149: The reference corresponding to the study mentioned on this sentence should be provided. Furthermore, this work also examines the impact on the emissions of the strict restrictions between the lockdown period and before, so how do the results presented in this study differ or complement the other study? Additionally, how do the estimated emissions compare between both studies.

Response: We have added a sentence there to explain that the analysis was performed for the 5 years prior to 2020.

Line 178: the weighted sum of squares of what? Please clarify.

Response: Sentence has been corrected (see Track Changes).

Line 182: Where is this number coming from? Are those the total number of observations for the period 2015 to 2020?

Response: This is the total number of observations from the 17 stations. If all stations do not have gaps, each station would have 8 measurements per day (we use 3h averaged measurements of aerosol absorption) for 31 (Jan) + 29 (Feb) + 31 (Mar) + 30 Apr = 121 days. This gives a total 968 measurements per station for the period January to April 2020. We have 15 dependent stations (plus 2 stations that we used for validation), so 14520 measurements in total. However, due to the gaps in the measurements due to screening or instrument failure, we always have less measurements. In our case, we had 12538 in total.

Line 267: Is the B matrix changed for each test according to the prior used or are the uncertainties of the prior emissions considered the same for all prior emissions? If not, how does the ïA¸cˇïAšïAaˇstatistic change for each test with a different prior?

Response: As we mention in section 2.3, we set uncertainties in each inversion in a way that we always get a x2 value equal to unity. Once we find the optimal uncertainties that result in x2=1, we use the same settings for each inversion with different priors. This gives consistency in our study, in the sense that we always give the same weight to observations and/or prior emissions. This is why, the resulting x2 values range between 0.8-1.5.

Line 283: Although country emissions might have decreased, figure 4 also shows an increase of emissions in center-south France. Also, please explain the geometry of the region with increased emissions over Poland. How can these straight lines be explained? What does it say about the inversion system?

Response: In Methods section, we explain that the different station measurements result in different average source-receptor matrices (SRMs) and, in turn, in different aggregated grids. To minimize the impact of using different station measurements (due to different data availability), we used exactly the same grid for the 2015-2019 and the 2020 inversions (see Figure 1), as otherwise differences in the posterior emissions can partly be due to different grid geometries.

This approach has some consequences. For instance, it results to regions with a high resolution grid-cells, despite that no measurements are available there (e.g., Poland). If we also check the prior emissions (Figure 3), we conclude that the high-

resolution grid in Poland is more strongly correlated to emission density than to emission sensitivity from the stations. This gives very much weight to the high emissions in Eastern Europe and less to the fact that emission sensitivities, there, are already quite low. And of course, there are somewhat more stations close to this area in 2015 than in 2020. We must admit that the rather poor data density for weekly timestep inversions push the method to the limit and one should be careful not to overinterpret the emission changes at smaller scales.
We have added a sentence in the Conclusions section to make this limitation clear to the readers.

Line 289: The authors should clearly state the difference in the number of stations used for the period 2015-2019 and the year 2020.

Response: We now explain this in the beginning of section 2.3 (see Track Changes).

Lines 302-303: Does this mean that the inversion was also conducted for each year since 2015 using the same stations as used in 2020? Doesn't this contradict what is said at the beginning of this section. Please clarify.

Response: The reviewer has a good point here. This sentence causes a misunderstanding; hence, we have reformulated it (p 13, Track Changes).

Line 353: I suppose that by "before" the authros refer to previous studies presented in the provided references. What do these results show? Is the impact associated to these other sources small compared to MAC? The authors should summarize the impact of the other sources on the inversion compared to the results obtained in this study?

Response: We have corrected this sentence as "…have been studied before and significantly smaller than the sources of uncertainty that are considered here (Evangeliou et al., 2018; Grythe et al., 2017)." See p.15 (Track Changes).

Line 354-355: Which period is considered in this analysis? Is it the entire period (2015-2020)? According to Figure 1, the network used changes between 2020 and the rest of the period. Given the uncertainty obtained it should be clarified which period is used.

Response: In this paper, we focus on the emissions of BC in 2020 and we only use emissions from previous years as an indication of how patterns in the 2020 emissions changed due to COVID-19 outbreak. Thus, the sensitivity of the emissions to the use of different MAC values for the conversion of absorption to eBC is only done for the 2020 emissions. We now give this detail in the relevant paragraph (see Track Changes in p14-15).

Line 356: How much does "increases dramatically" represent? Please reformulate.

Response: We added that the uncertainty can reach up to 100% far the observations (p 15, Track Changes).

Line 357: I do not think that "Accordingly" is the correct word to be used here. I suppose the tests were conducted independently by fixing the other parameters (ie, fixed emissions when testing uncertainty due to MAC).

Response: We have removed the word "accordingly" from the sentence. The reviewer has a good point here (p 15, Track Changes).

Line 363: Why were only two stations left out for the independent validation? Furthermore, both stations are located close to a station actually used in the inversion and since uncertainty "increases dramatically" far from the observations, using two "nearby" stations for validation represents the "best scenario" case. How independent are these two stations actually? How does the performance changes if isolated independent stations are used for validation?

Response: Since these observations were not included in the inversion to optimize emissions, then they are independent, by definition. The reason why we chose these 2 stations for our inversions is explained in p. 15 ("Due to the higher measurement station density … that lack observations."). For your consideration, we had 17 stations available, with a poor coverage in Europe; 2 of them are practically adjacent to others. This means that if we sacrificed stations for independent validation at the edges of our domain (i.e., in Italy, Norway or Spain) the surface area without measurements in our grid would increase. We think that it was the wisest solution to exclude stations where station density is high.

;

Line 367, Figure 7: Since the uncertainty is not included in the analysis below, I would suggest to remove the illustration from the error (MAC & Prior) in order to make the figure easier to read. In it's present state, it is difficult to identify the different lines.

Response: We believe it is important to show that posterior concentrations are associated with large uncertainties as shown in Figure 7. The better agreement of the posterior concentrations is proved by the statistics we show in the figure using the prior and posterior concentrations against observations. To improve the figure according to the reviewer's suggesting we have used more transparent colors for the uncertainties in posterior concentrations (see new Figure 7).

Lines 384-385: I have to admit I'm confused here. Figure 3 in the supplement shows that in all countries (except Scandinavia), MERRA-2 concentrations during lockdown in 2020 were not the lowest ones. How is this compatible with saying that and improved air quality was seen over Europe during lockdown based on MERRA-2 data?

Response: We have corrected this sentence to make it clear to the reader. MERRA concentrations generally decreased in Europe (as seen in the relevant figure at the bottom) since January 2020, and only after the lockdown was over, we saw a tendency to increase again. In addition, we also see the episodic (usually for no more than 1 week) peaks during the lockdown, that we think they are due to residential combustion.

Figure 8c: In figure caption please indicate the color used for each station.

Response: We have followed reviewer's suggestion and corrected the caption (see text with Track Changes).

Lines 414-421: I do not entirely agree with this analysis, Although the emissions were reduced in most selected countries, for France emissions for 2016 and 2018 were smaller than for 2020, at least for the first half of the lockdown period. Similarly, for Italy emissions in 2015 and 2017 were lower than for 2020. This is consistent with what is said at the beginning of section 4, where it is stated that increase light absorption mea- surement are observed at the beginning of the lockdown due to

increased residential emission. Isn't it contradictory what is stated at the end of section 4 with what is said a the beginning of the same section?

Response: In the beginning of section 4, we try to link the patterns of the 2020 emissions of BC with what is seen in MERRA-2 assimilated concentrations. At the end, of the section, we compare the 2020 emissions during the lockdown with what is seen for the 5 previous years. We have explained previously that difference in emissions during the whole study period for the different years cannot be attributed to the lockdown and is rather due to reported measurements that could be increased or decreased from year to year. However, the differences during the lockdown from the period before is what it is of interest here, as this shows the real impact of the lockdown. In 2020, a clear decrease was pronounced opposite or larger than in the previous years. We have tried to make this part more consistent in the text.

Changes in black carbon emissions over Europe due to COVID-19 lockdowns

Nikolaos Evangeliou[1,*], Stephen M. Platt[1], Sabine Eckhardt[1], Cathrine Lund Myhre[1], Paolo Laj[2,3,4], Lucas Alados-Arboledas[5,6], John Backman[7], Benjamin T. Brem[8], Markus Fiebig[1], Harald Flentje[9], Angela Marinoni[10], Marco Pandolfi[11], Jesus Yus-Dìez[11], Natalia Prats[12], Jean P. Putaud[13], Karine Sellegri[14], Mar Sorribas[15], Konstantinos Eleftheriadis[16], Stergios Vratolis[16], Alfred Wiedensohler[17], Andreas Stohl[18]

[1]Norwegian Institute for Air Research (NILU), Department of Atmospheric and Climate Research (ATMOS), Kjeller, Norway.
[2]University of Grenoble Alpes, CNRS, IRD, Grenoble-INP, IGE, 38000 Grenoble, France.
[3]CNR-ISAC, National Research Council of Italy – Institute of Atmospheric Sciences and Climate, Bologna, Italy.
[4]University of Helsinki, Atmospheric Science division, Helsinki, Finland.
[5]Andalusian Institute for Earth System Research (IISTA-CEAMA), Granada, Spain.
[6]Department of Applied Physics, University of Granada, Granada, Spain.
[7]Atmospheric Composition Research, Finnish Meteorological Institute, Helsinki, Finland.
[8]Laboratory of Atmospheric Chemistry, Paul Scherrer Institute, Villigen PSI, Switzerland.
[9]Deutscher Wetterdienst, Meteorologisches Observatorium Hohenpeissenberg, Albin-Schwaiger-Weg 10, 82383 Hohenpeissenberg, Germany.
[10]Institute of Atmospheric Sciences and Climate, National Research Council of Italy (ISAC-CNR), 40121, Bologna, Italy.
[11]Institute of Environmental Assessment and Water Research IDAEA-CSIC, C/Jordi Girona 18-26, Barcelona 08034, Spain.
[12]Izaña Atmospheric Research Center, State Meteorological Agency (AEMET), C/La Marina 20, 38001, Tenerife, Spain.
[13]European Commission, Joint Research Centre (JRC), Via Enrico Fermi 2749, Ispra (VA) 21027, Italy.
[14]Laboratoire de Météorologie Physique, UMR6016, CNRS/UBP, 63178 Aubière, France.
[15]El Arenosillo Atmospheric Sounding Station, Atmospheric Research and Instrumentation Branch, National Institute for Aerospace Technology, 21130 Huelva, Spain.

[16]Environmental Radioactivity Lab, Institute of Nuclear & Radiological Sciences & Technology, Energy & Safety, NCSR "Demokritos", Ag. Paraskevi, Athens, Greece.
[17]Department Experimental Aerosol and Cloud Microphysics, Leibniz Institute for Tropospheric Research, Leipzig, Germany.
[18]Department of Meteorology and Geophysics, University of Vienna, UZA II, Althanstraße 14, 1090 Vienna, Austria.

* Corresponding author: N. Evangeliou (Nikolaos.Evangeliou@nilu.no)

Abstract

Following the emergence of the severe acute respiratory syndrome coronavirus 2 (SARS-CoV-2) responsible for COVID-19 in December 2019 in Wuhan (China) and its spread to the rest of the world, the World Health Organization declared a global pandemic in March 2020. Without effective treatment in the initial pandemic phase, social distancing and mandatory quarantines were introduced as the only available preventative measure. In contrast to the detrimental societal impacts, air quality improved in all countries that strict lockdowns were applied, due to lower pollutant emissions. Here we investigate the effects of the COVID-19 lockdowns in Europe on ambient black carbon (BC), which affects climate and damages health, using in-situ observations from 17 European stations in a Bayesian inversion framework. BC emissions declined by 23 kt in Europe (20% in Italy, 40% in Germany, 34% in Spain, 22% in France) during lockdowns compared to the same period in the previous five years, which is partially attributed to COVID-19 measures. BC temporal variation in the countries enduring the most drastic restrictions showed the most distinct lockdown impacts. Increased particle light absorption in the beginning of the lockdown, confirmed by assimilated satellite and remote sensing data, suggests residential combustion was the dominant BC source. Accordingly, in Central and Eastern Europe, which experienced lower than average temperatures, BC was elevated compared to the previous five years. Nevertheless, an average decrease of 11% was seen for the whole of Europe compared to the start of the lockdown period, with the highest peaks in France (42%), Germany (21%), UK (13%), Spain (11%) and Italy (8%). Such a decrease was not seen in the previous years, which also confirms an impact of COVID-19 on the European emissions of BC.

Deleted: Despite the socioeconomic impacts

Deleted: 11%

Deleted: 32

Deleted: 20

Deleted:

Deleted: at

Deleted: Except for the comparison of BC emissions in the lockdown with the previous five years, an immediate decrease was also seen, as compared with the period before the lockdown, which averaged about 10% over Europe…

Deleted: BC

Deleted: from COVID-19

1 Introduction

The identification of the severe acute respiratory syndrome coronavirus 2 (SARS-CoV-2 or COVID-19) in December 2019 (WHO, 2020) in Wuhan (China) and its subsequent transmission to South Korea, Japan, and Europe (initially mainly Italy, France and Spain) and the rest of the world led the World Health Organization to declare a global pandemic by March 2020 (Sohrabi et al., 2020). Although the symptoms are normally mild or not even detected for most of the population, people with underlying diseases or elderly are very vulnerable showing complications that can lead to death (Huang et al., 2020). Considering the lack of available treatment and vaccination to combat further spread of the virus, the only prevention measures included strict social, travel and working restrictions in a so-called lockdown period that lasted for several weeks (mid-March to end of April 2020 for most of Europe). The most drastic measures were taken in China, where the outbreak started, in Italy that faced large human losses and later in the United States. Despite all these restriction, still six months after the first lockdown, several countries are reporting severe human losses due to the virus (John Hopkins University of Medicine, 2020).

Despite the dramatic health and socioeconomic consequences of COVID-19 lockdowns, their environmental impact might be beneficial. Bans on mass gatherings, mandatory school closures, and home confinement (He et al., 2020; Le Quéré et al., 2020) during lockdowns have all resulted in lower traffic-related pollutant emissions and improved air quality in Asia, Europe and America (Adams, 2020; Bauwens et al., 2020; Berman and Ebisu, 2020; Conticini et al., 2020; Dantas et al., 2020; Dutheil et al., 2020; He et al., 2020; Kerimray et al., 2020; Le et al., 2020; Lian et al., 2020; Otmani et al., 2020; Sicard et al., 2020; Zheng et al., 2020). The restrictions also present an opportunity to evaluate the cascading responses from the interaction of humans, ecosystems, and climate with the global economy (Diffenbaugh et al., 2020).

Strongly light absorbing black carbon (BC, or 'soot'), is produced from incomplete combustion of carbonaceous fuels e.g. fossil fuels, wood burning, biofuels (Bond et al., 2013). By absorbing solar radiation, it warms the air, reduces tropical cloudiness (Ackerman, 2000) and atmospheric visibility (Jinhuan and Liquan, 2000). BC causes pulmonary diseases (Wang et al., 2014a), may act as cloud condensation nuclei affecting cloud formation and precipitation (Wang et al., 2016) and contributes to global warming (Bond et al., 2013; Myhre et al., 2013; Wang et al., 2014a). When deposited on snow, it reduces snow albedo (Clarke and Noone, 1985; Hegg et al., 2009) accelerating melting. Since BC is both climate relevant and strongly

Field Code Changed
Formatted: Norwegian Bokmål
Formatted: Norwegian Bokmål

linked to anthropogenic activity, it is important to determine the effects of the COVID-19 lockdowns thereon.

Here, we present a rigorous assessment of temporal and spatial changes BC emissions over Europe (including Middle East and parts of North Africa), combining in situ observations from the Aerosol, Clouds and Trace Gases Research Infrastructure (ACTRIS) network and state-of-the-art emission inventories within a Bayesian inversion. We validate our results with independent satellite data and compare them to inventories and baseline and optimized emissions calculated for previous years.

2 Methods

This section gives a detailed description of all datasets and methods used for the calculation of COVID-19 impact. Section 2.1 describes the instrumentation of the particle light absorption measurements from Aerosol, Clouds and Trace Gases Research Infrastructure (ACTRIS), and the networks European Monitoring and Evaluation Program (EMEP) and Global Atmosphere Watch (GAW). These measurements were used in the inverse modelling algorithm (dependent measurements) and to validate the optimised (posterior) emissions of BC (independent measurements). For each of the observations and stations, the source – receptor matrices (SRMs), also known as "footprint emission sensitivities" or "footprints", were calculated as described in section 2.2. The latter together with the observations were fed in the inversion algorithm described in section 2.3. To overcome classic inverse problems (Tarantola, 2005), prior (a priori) emissions of BC were used in the inverse modelling algorithm calculated using bottom-up approaches (section 2.4). The optimised (a posteriori) emissions of BC were compared with reanalysis data from MERRA-2 (Modern-Era Retrospective Analysis for Research and Applications Version 2), which are described in section 2.5, while MERRA-2 Ångström exponent data together with absorption Ångström exponent from the aerosol robotic network (AERONET) (section 2.6) were used to examine the presence of biomass burning aerosols in Europe. A description of the statistical tests and the country definitions used in the paper is given in sections 2.7 and 2.8, respectively.

2.1 Particle light absorption measurements

The measurement sites contributing data to this paper are regional background sites (except for one site in Germany) and all contribute to the research infrastructure ACTRIS, and the networks EMEP and GAW. The measurement data used for the period 2015 - May 2020 consist of hourly-averaged, quality-checked, particle light absorption measurements. The

Formatted: Normal, Justified, Indent: First line: 1 cm

Formatted: Font colour: Auto

Deleted: Aerosol, Clouds and Trace Gases Research Infrastructure (…

Deleted:)

Deleted: European Monitoring and Evaluation Program (

Deleted:)

Deleted: Global Atmosphere Watch (

Deleted:)

quality assurance and quality control correspond to the Level 2 requirements for ACTRIS, EMEP and GAW data, as described in detail in Laj et al. (2020).

All absorption measurements within ACTRIS and EMEP are taken using a variety of filter-based photometers: Multi-Angle Absorption Photometers (MAAP), Particle Soot Absorption Photometers (PSAP) Continuous Light Absorption Photometers (CLAP), and the Aethalometer (AE31). Information on instrument type at the various sites are included in Table 1, and procedures for harmonization of measurement protocols to produce comparable data seta are described in Laj et al. (2020) in detail. Zanatta et al. (2016) suggested that a mass absorption cross-section (MAC) value of 10 m^2 g^{-1} (geometric standard deviation of 1.33) at a wavelength of 637 nm can be considered to be representative of the mixed boundary layer at European ACTRIS background sites, where BC is expected to be internally mixed to a large extent. Assuming an absorption Ångström exponent (AAE) is equal to unity, i.e. assuming no change in MAC for different sources (Zotter et al., 2017), we extrapolated the MACs at 637 nm ($MAC_{@\lambda 1}$) to the measurement wavelengths of our study ($MAC_{@\lambda 2}$) using the following equation:

$$MAC_{@\lambda 2} = MAC_{@\lambda 1}\left(\frac{\lambda 1}{\lambda 2}\right)^{AAE} \xrightarrow{yields} MAC_{@\lambda 2} = 10\left(\frac{637}{\lambda 2}\right)^{1} \quad (1)$$

following Lack and Langridge (2013). The resulting MAC values for each measurement station are shown in Table 1.

2.2 Source – receptor matrix (SRM) calculations

SRMs for each of the 17 receptor sites (Table 1) were calculated using the Lagrangian particle dispersion model FLEXPART version 10.4 (Pisso et al., 2019). The model releases computational particles that are tracked backward in time based on 3-hourly operational meteorological analyses from the European Centre for Medium-Range Weather Forecasts (ECMWF) with 137 vertical layers and a horizontal resolution of 1°×1°. The tracking of BC particles includes gravitational settling for spherical particles with an aerosol mean diameter of 0.25 µm and a logarithmic standard deviation of 0.3 and a particle density of 1500 kg m^{-3} (Long et al., 2013). FLEXPART also simulates dry and wet deposition (Grythe et al., 2017), turbulence (Cassiani et al., 2014), unresolved mesoscale motions (Stohl et al., 2005) and includes a deep convection scheme (Forster et al., 2007). SRMs were calculated for 30 days backward in time, at temporal intervals that matched measurements at each receptor site. This backward tracking is sufficiently long to include almost all BC sources that contribute to surface

Deleted: Table 1

Deleted: Table 1

Deleted: Source – receptor matrices (

Deleted:), also known as “footprint emission sensitivities” or “footprints”…

Deleted: Table 1

concentrations at the receptors given a typical atmospheric lifetime of 3–11 days (Bond et al., 2013).

2.3 Bayesian inverse modelling

The Bayesian inversion framework FLEXINVERT+ described in detail in Thompson and Stohl (2014) was used to optimize emissions of BC before (January to mid-March 2020) and during the COVID-19 lockdown period in Europe (mid-March to end of April 2020). To show potential differences on the signal from the 2020 restrictions, emissions were optimised with the same set up during the same period (January to April) in the previous five years (2015–2019). Note that the number of stations in the inversions of 2015–2019 was slightly higher (20 stations against 15 that were used in 2020), due to different data availability. The algorithm finds the optimal emissions, which lead to FLEXPART modelled concentrations that better match the observations considering the uncertainties for observations, prior emissions and SRMs. Specifically, the state vector of BC concentrations, $y^{mod}_{(M\times1)}$, at M points in space and time can be modelled given an estimate of the emissions, $\boldsymbol{x}_{(N\times1)}$, of the N state variables discretised in space and time, while atmospheric transport and deposition are linear operations described by the Jacobian matrix of SRMs, $\mathbf{H}_{(M\times N)}$:

$$y^{mod} = \mathrm{H}x + \epsilon \qquad (2)$$

where ϵ is an error associated with model representation, such as the modelled transport and deposition or the measurements. Since H is not invertible or may not have unique inverse, according to Bayesian statistics, the inverse problem can be described as the maximization of the probability density function of the emissions given the prior information and observations. This is equivalent to the minimun of the cost function:

$$\mathbf{J}(\boldsymbol{x}) = \frac{1}{2}(\boldsymbol{x}-\boldsymbol{x_b})^{T}\mathbf{B^{-1}}(\boldsymbol{x}-\boldsymbol{x_b}) + \frac{1}{2}(\boldsymbol{y}-\mathbf{H}\boldsymbol{x})^{T}\mathbf{R^{-1}}(\boldsymbol{y}-\mathbf{H}\boldsymbol{x}) \qquad (3)$$

where $\boldsymbol{y}$ is the vector of observed BC concentrations, $\boldsymbol{x}$ and $\boldsymbol{x_b}$ the vectors of optimized and prior emissions, respectively, while **B** and **R** are the error covariance matrices that weight the posterior–prior flux and observation–model mismatches, respectively. Based on the Bayes' theorem, the most probable posterior emissions, $\boldsymbol{x}$ are given by the following equation (Tarantola, 2005):

$$\boldsymbol{x} = \boldsymbol{x_b} + \mathbf{BH^{T}}(\mathbf{HBH^{T}} + \mathbf{R})^{-1}(\boldsymbol{y} - \mathbf{H}\boldsymbol{x_b}) \qquad (4)$$

Here, posterior emissions were calculated weekly between 1 January and 30 April 2020. The aggregated inversion grid (25°N–75°N and 10°W–50°E) and the average SRM for inversions are shown in Figure 1, while the measurement stations are listed in Table 1. The

Moved (insertion) [1]

Deleted: , we calculated the posterior emissions of BC for the same periods in the years 2015–2019. …

Deleted: -

Formatted: Font: Not Bold

Formatted: Font: Not Bold

Formatted: English (US)

Formatted: Indent: First line: 0 cm

Deleted: The optimized (a posteriori) emissions are those that

Deleted: ize

Formatted: Font: Font colour: Auto, English (US)

Deleted: 2

Deleted: where **H** is the Jacobian matrix of SRMs

Deleted: ,

Deleted: for the prior emissions and the observations

Deleted: The

Deleted: 3

Moved up [1]: To show potential differences on the signal from the 2020 restrictions, we calculated the posterior emissions of BC for the same periods in the years 2015–2019.

Deleted: Figure 1

Deleted: Table 1

variable grid uses high resolution at regions, where there are many stations and hence strong contribution from emissions, while it lowers resolution at regions that lack measurement stations following a method proposed by Stohl et al. (2010).

Prior emission errors **B** are correlated in space and time, but very little is known about the true temporal and spatial error correlation patterns. The spatial error correlation for the emissions is defined as an exponential decay over distance (we assume that emissions on land and ocean are not correlated). The temporal error correlation matrix is described similarly using the time difference between grid cells in different time steps. The full temporal and spatial correlation matrix is given by the Kronecker product (see Thompson and Stohl, 2014). The error covariance matrix for the emissions is the matrix product of correlation pattern and the error covariance of the prior fluxes. We calculate the error on the emissions in each grid-cell (on the fine grid) as a fraction of the maximum value out of that grid cell and the eight surrounding ones.

The observation error covariance matrix **R** combines measurement, transport model and representation errors. For the measurement errors, we use values given by the data providers. Transport model errors are difficult to quantify and depend not only on the model but also on the meteorological inputs. Therefore, we do not quantify the full transport error, but only the part of it that can be estimated from FLEXPART, i.e. the stochastic uncertainty (see Stohl et al., 2005). As regards to representation errors, we consider observation representation error and model aggregation error. The observation representation error is calculated from the standard deviation of all measurements available in a user-specified measurement averaging time interval, based on the idea that if the measurements are fluctuating strongly within that interval then their mean value is associated with higher uncertainty than if the measurements are steady (Bergamaschi et al., 2010). The aggregation error is attributed to reduction of the spatial resolution of the model and is calculated by projecting the loss of information in the state space into the observation space (Kaminski et al., 2001). Hence, the observation error covariance matrix is defined as the diagonal matrix with elements equal to the quadratic sum of the measurement, transport model and measurement representation errors (Thompson and Stohl, 2014).

Theoretically, the algorithm can calculate negative posterior emissions, which are physically unlikely. To tackle this problem, an inequality constraint was applied on the emissions following the method of Thacker (2007) that applies the constraint as "error-free" observations:

$$\boldsymbol{x} = \boldsymbol{x} + \mathbf{A}\mathbf{P}^{\mathbf{T}}(\mathbf{P}\mathbf{A}\mathbf{P}^{\mathbf{T}})^{-1}(\boldsymbol{c} - \mathbf{P}\boldsymbol{x}) \qquad (5)$$

Deleted: 4

where **A** is the posterior error covariance matrix, **P** is a matrix operator to select the variables that violate the inequality constraint, and $\boldsymbol{c}$ is a vector of the inequality constraint, which in this case is zero.

We evaluated the assumptions made on the error covariance matrices for the prior emissions and the observations using the reduced χ^2 statistics (**B** and **R**). When χ^2 is equal to unity, the posterior solution is within the limits of the prescribed uncertainties. The latter is the value of the cost function at the optimum (Thompson et al., 2015). In the inversions performed here, the calculated χ^2 values were between 0.8 and 1.5 indicating that the chosen uncertainty parameters are close to the ideal ones. The number of measurements used in each inversion was equal to 12538 from 17 stations. To select the inversion that provides the most statistically significant result, an evaluation of the improvement in the posterior modelled concentrations, with respect to the prior ones, against the observations was performed (Figure 2). The resulting values of each of the statistical measures that were performed are given in detail in Table 2. Note that this is not a validation of the posterior emissions, because the comparison is only done for the observations that were included in the inversion (dependent observations), and the inversion algorithm has been designed to reduce the model–observation mismatches. This means that the reduction of the posterior concentration mismatches to the observations is determined by the weighting that is given to the observations with respect to the prior emissions. A proper validation of the posterior emissions is performed against observations that were not included in the inversion (independent observations) in section 3.3.

Deleted: and is equivalent to the weighted sum of squares divided by the number of observations …

Deleted: Figure 2

Deleted: Table 2

Deleted: Results

2.4 Prior emissions

As a priori emissions in the inversions, the ECLIPSE version 5 and 6 (Evaluating the CLimate and Air Quality ImPacts of ShortlivEd Pollutants) (Klimont et al., 2017), EDGAR (Emissions Database for Global Atmospheric Research) version HTAP_v2.2 (Janssens-Maenhout et al., 2015), ACCMIP (Emissions for Atmospheric Chemistry and Climate Model Intercomparison Project) version 5 (Lamarque et al., 2013) and PKU (Peking University) (Wang et al., 2014b) were used (Figure 3). All inventories include the basic emission sectors (e.g., waste burning, industrial combustion and processing, all means of transportation (aerial, surface, ocean), energy conversion, residential and commercial combustion (see references therein). Biomass burning emissions were adopted from the Global Fire Emissions Database, Version 4.1s (GFEDv4.1s)(Giglio et al., 2013).

Deleted: ref

Deleted: Figure 3

2.5 MERRA-2 (Modern-Era Retrospective Analysis for Research and Applications Version 2)

The MERRA-2 reanalysis dataset for BC (Randles et al., 2017) assimilates bias-corrected AOD from Moderate Resolution Imaging Spectroradiometer (MODIS), Advanced Very High Resolution Radiometer (AVHRR) instruments, Multiangle Imaging SpectroRadiometer (MISR) and Aerosol Robotic Network (AERONET) with the Goddard Earth Observing System Model Version 5 (GEOS-5). BC and other aerosols in MERRA-2 are simulated with the Goddard Chemistry, Aerosol, Radiation and Transport (GOCART) model and delivered in hourly to monthly temporal resolution and 0.5°×0.625° spatial. The product has been validated for AOD, PM and BC extensively (Buchard et al., 2017; Qin et al., 2019; Randles et al., 2017; Sun et al., 2019). Ångström exponent (AE), a measure of how the AOD changes relative to the various wavelength of light, is derived here from AOD469, AOD550, AOD670, and AOD865, by fitting the data to the linear transform of Ångström's empirical expression:

$$\tau_\lambda = \tau_{\lambda_0}(\frac{\lambda}{\lambda_0})^{-a} \qquad (6)$$

where τ_λ is the known AOD at wavelength λ (in nm), τ_{λ_0} is the AOD at 1000 nm, and α stands for AE (Gueymard and Yang, 2020).

2.6 Absorption Ångström exponent from Aerosol Robotic Network (AERONET) data

Aerosol composition over Europe during the COVID-19 lockdown was confirmed using the AERONET data (Holben et al., 1998). AERONET provides globally distributed observations of spectral aerosol optical depth (AOD), inversion products, and precipitable water in diverse aerosol regimes. The AE for a spectral dependence of 440-870 nm is related to the aerosol particle size. Values less than 1 suggest an optical dominance of coarse particles corresponding to dust, ash and sea spray aerosols, while values greater than one imply dominance of fine particles such as smoke and industrial pollution (Eck et al., 1999). We chose data from five stations covering Western, Central and Eastern Europe, for which cloud-free measurements exist for the lockdown period, namely Ben Salem (9.91°E, 35.55°N), Minsk (27.60°E, 53.92°N), Montsec (0.73°E, 42.05°N), MetObs Lindenberg (14.12°E, 52.21°N) and Munich University (11.57°E, 48.15°N). We used Level 1.5 absorption AE (AAE) measurements for the COVID-19 lockdown period (14 March to 30 April 2020).

Field Code Changed

Deleted: 5

Deleted: AErosol

Deleted: RObotic

Deleted: ET

2.7 Statistical measures

For the performance evaluation of the inversion results against dependent (observations that were included in the inversion) and independent observations (observations that were not included in the inversion), four different statistical quantities were used:

(1) Pearson's correlation coefficient:

$$R_{mo} = \frac{n\sum_{i=1}^{n} m_i o_i - \sum_{i=1}^{n} m_i \sum_{i=1}^{n} o_i}{\sqrt{n\sum_{i=1}^{n} m_i^2 - (\sum_{i=1}^{n} m_i)^2}\sqrt{n\sum_{i=1}^{n} o_i^2 - (\sum_{i=1}^{n} o_i)^2}} \quad (7)$$

where n is sample size, m and o the individual sample points for model concentrations and observations indexed with i.

(2) The normalized root mean square error (nRMSE):

$$nRMSE = \frac{\sqrt{\sum_{i=1}^{n} \frac{1}{n}(m_i - o_i)^2}}{o_i^{max} - o_i^{min}} \quad (8)$$

(3) The mean fractional bias MFB was selected as a symmetric performance indicator that gives equal weights to under- or over-estimated concentrations (minimum to maximum values range from -200% to 200%) and is defined as:

$$MFB = \frac{1}{n}\frac{\sum_{i=1}^{n}(m_i - o_i)}{\sum_{i=1}^{n}(\frac{m_i + o_i}{2})} \quad (9)$$

(4) The mean absolute error was computed normalized ($nMAE$) over the average of all the actual values (observations here), which is a widely used simple measure of error:

$$nMAE = \frac{\sum_{i=1}^{n}|m_i - o_i|}{\sum_{i=1}^{n} o_i} \quad (10)$$

2.8 Region definitions

All country and regional masks are publicly available. Regions used for statistical processing purposes were adopted from the United Nations Statistics Division (https://unstats.un.org/home/). Accordingly, Northern Europe includes UK, Norway, Denmark, Sweden, Finland, Iceland, Estonia, Latvia and Lithuania. Southern Europe includes Spain, Italy, Greece, Slovenia, Croatia, Bosnia, Serbia, Albania and North Macedonia. Western Europe is defined by France, Belgium, Holland, Germany, Austria and Switzerland. Eastern Europe includes Poland, Czechia, Slovakia, Hungary, Romania, Bulgaria, Moldova, Ukraine, Belarus and Russia.

Deleted: 6

Deleted: 7

Deleted: 8

Deleted: 9

3 Results

3.1 Optimized (posterior) emissions from Bayesian inversion

We performed five inversions for BC over Europe for 1st January- 30th April 2020, each with different prior emissions from ECLIPSE version 5 and 6, EDGAR version HTAP_v2.2, ACCMIP version 5 and PKU (Figure 3). Total prior emissions of BC in Europe from the five emission inventories for the period of the inversion ranged between 192-377 kt. We evaluated the assumptions made on the error covariance matrices for the prior emissions and the observations using the reduced χ^2 statistic (**B** and **R**, see section 2.3). When χ^2 is equal to unity, the posterior solution is within the limits of the prescribed uncertainties. The performance of the inversions with the five different prior inventories was evaluated using four statistical parameters (see section 2.7). The best performance of the inversions was achieved using ECLIPSEv6 (Table 2 and Figure 2) with the smallest $nRMSE$ (0.073) value, the largest Pearson's R^2 (0.60), the closest to zero MFB value (0.03) and the smallest $nMAE$ (714). Therefore, all the results presented below correspond to this inversion.

Posterior emissions of BC were calculated to be 191 kt in the inversion domain (10°W–50°E, 25°N–75°N) or approximately 20% smaller than those in ECLIPSEv6 (239 kt) (Figure 4). Note that these numbers refer to the whole inversion domain (not only Europe) and the whole study period (January – April 2020). The largest posterior differences were found in the eastern part of the domain (20°E–50°E, 45°N–55°N), where emissions dropped from 35 to 29 kt. Emissions of BC in the western part of the inversion domain (10°W–20°E, 45°N–55°N) declined by almost 11% (from 45 to 40 kt), as those in the north part (5°W–35°E, 55°N–70°N) that covers Scandinavian countries (from 8.7 to 6.4 kt). Finally, in the southern part (10°W–50°E, 35°N–45°N) of the domain (Spain, Italy, Greece) the posterior emissions also decreased by 21% relative to the priors (from 61 to 48 kt). The largest country decreases were seen in France (from 14 to 8.2 kt), Italy (from 8.0 to 5.9 kt), UK (from 4.4 to 3.1 kt) and Germany (from 4.5 to 4.1 kt). Surprisingly, BC emissions were slightly enhanced in Poland (from 21 to 23 kt), and in Spain (from 6.3 to 7.5 kt). In general, inversion algorithms reduce the mismatches between modelled concentrations and observation by correcting emissions (section 2.3). If decreased posterior emissions are calculated during the whole inversion period (before and during the lockdowns), impact from the COVID-19 restrictions cannot be concluded and, most likely, the reduced emissions are due to errors in the prior emissions. In the next section (3.2), we demonstrate that this decrease was due to the COVID-19 lockdowns, by comparing

Deleted: Figure 3
Deleted: Table 2
Deleted: Figure 2
Deleted: Emissions
Deleted: Figure 4
Deleted: aforementioned
Deleted: decreases
Deleted: Eastern Europe
Deleted: Western European e
Formatted: Not Highlight
Formatted: Not Highlight
Formatted: Not Highlight
Formatted: Not Highlight
Formatted: Not Highlight
Deleted: Southern Europe
Formatted: Not Highlight
Formatted: Not Highlight
Deleted: were slightly enhanced
Deleted: Note that although posterior
Deleted: may only imply
Deleted: ,
Deleted: e
Deleted: in fact

posterior emissions with emissions from previous years, as well as with the respective emissions before and during the lockdown measures.

3.2 Comparison with previous years

We also performed inversions for 2015–2019 for the same period as the 2020 lockdowns (January- April) using almost the same measurement stations and keeping the same settings. The difference in BC emissions during the lockdown in 2020 (14 March to 30 April) from the respective emissions during the same period in 2015–2019 (14 March to 30 April) are shown in Figure 5 (a, emission anomaly) together with the gross domestic product (GDP) (Kummu et al., 2020) (b) , and (c) temperature anomaly from ERA-5 (Copernicus Climate Change Service (C3S), 2020) for the same period as the emission anomaly. The difference in the 2020 emissions of BC during the lockdown from the respective emissions in the same period in each of the previous years (2015–2019) is illustrated in Supplementary Figure 1. As an independent source of information, active fires from MODIS satellite product MCD14DL (Giglio et al., 2003) are also shown in Figure 5a and Supplementary Figure 1.

Overall, BC emissions decreased by ~46 kt during the COVID-19 lockdown in the inversion domain (10°W–50°E, 25°N–70°N) as compared with the same period in the previous five years. We record a significant decrease in BC emissions in Central Europe (Northern Italy, Austria, Germany, Spain and some Balkan countries) (Figure 5). On average, emissions were 23 kt lower (63 to 40 kt) over Europe during the lockdown in 2020 than in the same period of 2015–2019 (Figure 5). The decrease has the same characteristics when compared to each of previous years since 2015 (Supplementary Figure 1) based on measurements of BC at similar regions as those used for the 2020 inversion. The countries that showed drastic reductions in BC emissions during the lockdowns were those that suffered from the pandemic dramatically, with many human losses, strict social distancing rules and consequently less transport. Specifically, comparing with the previous five years, the 2020 emissions of BC during the lockdowns dropped by 20% in Italy (3.4 to 2.7 kt), 40% in Germany (3.3 to 2.0 kt), 34% in Spain (4.7 to 3.1 kt), 22% in France (3.5 to 2.7 kt) and remained the same or were slightly enhanced in Poland (~9.2 kt), and Scandinavia (~1.2 kt). Overall, BC emissions during the 2020 lockdowns in Western Europe declined by 32% (8.8 to 6.0 kt), in Southern Europe by 42% (17 to 9.9 kt) and in Northern Europe by 29% (5.4 to 3.8 kt) as compared with the 2015–2019 period. BC emissions in Eastern Europe were slightly increased during the 2020 lockdown as compared to the same period in the last five years (28 to 31 kt). The hot-spot emissions in Eastern Europe coincide with the presence of active fires as revealed from MODIS (Figure 5a).

Deleted: in the next section (3.2).

Deleted: Figure 5

Deleted: Supplementary Figure 1

Deleted: 48

Deleted: Figure 5

Deleted: compared to the same period during the last five years…

Deleted: declined from

Deleted: 44

Deleted: 39

Deleted: Supplementary Figure 1

Deleted: the same stations

Deleted: 2

Deleted: 0

Deleted: 2.2

Deleted: 1.3

Deleted: 23

Deleted: 3

Deleted: .4

Deleted: 2

Deleted: 6

Deleted: 7.0

Deleted: France (~2.2 kt)

Deleted: 2

Deleted: 22

Deleted: 6.2

Deleted: 4.8

Deleted: 36

Deleted: 12

Deleted: 7.7

Deleted: 26

Deleted: 3.8

Deleted: 2

Deleted: 22

Deleted: 24

Note that these numbers correspond to BC emissions during the COVID-19 lockdown period only (mid-March – April 2020).

Some localised areas of increased BC emissions exist in Southern France, Belgium, Northern Germany and Eastern Europe (Figure 5), which are observed relative to almost every year since 2015 (Supplementary Figure 1). While some hotspots in France cannot be easily explained, increased emissions in Eastern European countries are likely due to increased residential combustion, as people had to stay home during the lockdown. The combination of the financial consequences of the COVID-19 lockdown with the relatively low GDP per capita in these countries and the fact that from mid-March to end of April 2020 surface temperatures in these countries were significantly lower than in previous years is suggestive of increased emissions due to residential combustion. This source is most important in Eastern Europe (Klimont et al., 2017). Although residential combustion can be performed for heating or cooking needs in poorer countries, it is also believed to provide a more natural type of warmth and a comfortable and relaxing environment. Hence, it should not be assumed as an emission source in countries with lower GDPs only, especially as people spent more time at home. Moreover, the prevailing average temperatures over Europe during the lockdown were below 15°C (Supplementary Figure 2), a temperature used as a basis temperature below which residential combustion increases (Quayle and Diaz, 1980; Stohl et al., 2013).

Deleted: Figure 5

Deleted: Supplementary Figure 1

Deleted: Supplementary Figure 2

3.3 Uncertainty and validation of the posterior emissions

One of the basic problems when dealing with inverse modelling is that changing model, observational, or prior uncertainties can have drastic impacts on posterior emissions. We addressed this issue by finding the optimal parameters, in order to have a reduced χ^2 statistic around unity (see section 2.3). However, there are two other sources of uncertainty that, although not linked with the inversion algorithm, could affect posterior emissions drastically. The first is the use of different prior emissions; to estimate this type of uncertainty, we performed five inversions for January to April 2020 using each of the prior emission datasets (ECLIPSEv6 and v5, EDGAR_HTAPv2.2, ACCMIPv5 and PKU). The uncertainty was calculated as the gridded standard deviation of the posterior emissions resulting from the five inversions. The second type of uncertainty concerns measurement of BC, which is defined as a function of five properties (Petzold et al., 2013). However, as of today, no single instrument exists that could measure all of these properties at the same time. Hence, BC is not a single particle conistuent, rather an operational definition depending on the measurement technique (Petzold et al., 2013). Here we use light absorption coefficients (Petzold et al., 2013) converted

to equivalent BC (eBC) using the mass absorption cross section (MAC). The MAC is instrument specific and wavelength dependent. The site-specific MAC values used to convert the filter-based light absorption to eBC can be seen in Table 1. It has been reported that MAC values vary from 2 – 3 m^2 g^{-1} up to 20 m^2 g^{-1} (Bond and Bergstrom, 2006). To estimate the uncertainty of the posterior fluxes associated with the variable MAC, we performed a sensitivity study for January to April 2020 using MAC values of 5, 10 and 20 m^2 g^{-1} in all stations, as well as variable MAC values for each station (Table 1). Since these values are lognormally distributed, the uncertainty is calculated as the geometric standard deviation. The impact of other sources of uncertainty, such as those referring to scavenging coefficients, particle size and density that are used in the model have been studied before and significantly smaller than the sources of uncertainty that are considered here (Evangeliou et al., 2018; Grythe et al., 2017).

The posterior emissions are less sensitive to the use of different MACs than the use of different prior inventories (Figure 6). The relative uncertainty due to different use of MAC values was up to 20–30% in most of Europe and increases dramatically (~100%) far from the observations. The emission uncertainty of BC from the use of different priors was estimated to be up to 40% in Europe and shows very similar characteristics (same hot-spot regions and larger values where measurements lack). Overall, the combined uncertainty of BC emissions was ~60% in Europe.

Validation of top-down emissions obtained by inversion algorithms can be proper only if measurements that were not included in the inversion are to be used (independent observations). For this reason, we left out of the inversion observations from two stations (DE0054K and DE0066R, Table 1). Due to the higher measurement station density in Central Europe, we randomly selected two German stations, rather than from a country that is adjacent to regions that lack observations.

The prior, optimized and measured concentrations are shown in Figure 7 together with MERRA-2 surface BC concentrations at the same stations. The average footprint emission sensitivities are also given for the period of the lockdown. At station DE0054K, prior emissions represent observations very well until the beginning of the lockdown and then fail (Figure 7). On the other hand, the posterior emissions represent the variant concentrations during the lockdown effectively and also manage to capture some concentration peaks, which is reflected by lower $nRMSE$. Backward modelling showed that the enhanced concentrations originate from Northern Germany and the Netherlands, where posterior emissions were increased compared with the prior ones (Figure 4). A similar pattern was seen at station DE0066K,

Deleted: Table 1

Deleted: s

Deleted: Table 1

Deleted: Figure 6

Deleted: Accordingly, t

Deleted: Table 1

Deleted: Figure 7

Deleted: Figure 7

Deleted: Figure 4

although this station showed concentrations up to 4 mg m^{-3} (Figure 7). Again, the optimized emissions managed to represent the peaks at the end of January 2020 and at the beginning of the lockdown, which is again reflected by a half $nRMSE$ values and MFB close to zero as compared to the priors. The larger concentrations during the lockdown result from increased emissions over Eastern Germany, Poland and the Netherlands, as well as in oil industries in the North Sea (Figure 4b). In all these regions the footprint emissions sensitivities corresponding to the two independent stations were the highest.

4 Discussion

The improved air quality that Europe during the lockdown was also evident from the assimilated MERRA-2 satellite-based BC data. The latter are plotted in Supplementary Figure 3 (left axis) for 2015–2020, together with the posterior emissions calculated in the present study (right axis). For instance, weekly average concentrations of BC over Europe in MERRA-2 (Supplementary Figure 3, bottom). Many of the ACTRIS stations reported increased light absorption in the beginning of the lockdown (e.g., Figure 7); MERRA-2 data show the same patterns in France, Italy, UK and in Spain, and in all of Europe, in general. This can be explained by residential combustion considering that the surface temperature during the lockdown was lower than in previous years (Figure 5). The latter was confirmed by MERRA-2 reanalysis Ångström Exponent (AE) parameter at 470–870 nm, which shows higher values over Central and Eastern Europe during the lockdown in 2020 than in the same period of the previous years (Figure 8a,b). Larger AE values confirm the presence of wood burning aerosols (Eck et al., 1999). The fact that during the COVID-19 lockdown, residential combustion was a significant aerosol source in Europe, as compared to the previous years, was also confirmed by real-time observations of absorption AE from the AERONET data in five selected stations over Europe (Figure 8c). Measured absorption AE was higher during mid-March to April 2020 than in the same period of the last five years.

Emissions of BC calculated with Bayesian inversion for the lockdown period dropped substantially in most of the countries that suffered from further spread of the virus and, accordingly, from strict lockdown measures, as compared to the respective emissions before the lockdowns (Supplementary Figure 3). Specifically, the decrease in France was as high as 42%, 8% in Italy, 21% in Germany, 11% in Spain and 13% in the UK. Emissions also declined in Scandinavia by 5%, although Sweden did not enforce a lockdown. Overall, a reduction in BC emissions of about 11% can be concluded for Europe as a whole due to the lockdown.

Deleted: Figure 7
Deleted: Figure 4
Deleted: experienced
Deleted: Supplementary Figure 3Supplementary Figure 3
Deleted: ,
Deleted: between 2015–2020
Deleted: Figure 7
Deleted: Figure 5
Deleted: Figure 8
Deleted: Figure 8
Deleted: in the
Deleted: beginning of 2020
Deleted: Supplementary Figure 3
Deleted: 40
Deleted: 11
Deleted: 32
Deleted: 15
Deleted: 25
Deleted: 12
Deleted: 10

Stronger decreases in Eastern Europe were likely partly compensated by increased residential combustion in resulting from the prevailing low temperatures.

We report a 23 kt decrease in BC emissions in Europe during the lockdown that partially resulted from the COVID-19 outbreak, as compared to the same period in all previous years since 2015, based on particle light absorption measurements. We highlight these changes in BC emissions partially as a result of COVID-19 restrictions by plotting the temporal variability of the BC emissions in the 5 previous years (2015 – 2019) for France, Italy, Germany, Spain, Scandinavia and Europe (Figure 9). We record decreases in BC emissions in France, Italy, Germany and Scandinavia in mid-March to April 2020, opposite to what was estimated for all years between 2015 and 2019, which is obviously due to COVID-19. The UK and Spain showed a similar decrease in mid-March to April 2020 emissions as in all previous years (2015–2019). However, the estimated posterior BC emissions during the 2020 lockdowns were significantly lower than those of the same period in any of the previous years. Overall, emissions declined by 20% in Italy, 40% in Germany, 34% in Spain, 22% in France and remained the same and slightly enhanced in Scandinavia or Poland as compared to those of the last five years.

5 Conclusions

The impact of the COVID-19 lockdowns over Europe on the BC emissions, in response to the pandemic was assessed in the present manuscript. Particle light absorption measurements from 17 ACTRIS stations all around Europe were rapidly gathered and cleaned to produce a high-quality product. The latter was used in a well-established Bayesian inversion framework and BC emissions were optimised over Europe to better capture the observations. However, one should be careful not to overinterpret the emission changes at regional scales, due to the poor station data density used and the high resolution timesteps of the inversions (weekly posterior emissions). We calculate that the optimised (posterior) BC emissions declined from 63 to 40 kt (23%) during the lockdowns over Europe, as compared to the same period in the previous five years (2015–2019). The largest reductions were calculated for countries that suffered from the pandemic dramatically, such as Italy (3.4 to 2.7 kt), Germany (3.3 to 2.0 kt), Spain (4.7 to 3.1 kt), France (3.5 to 2.7 kt). BC emissions in Western Europe during the 2020 lockdowns were decreased from 8.8 to 6.0 kt (32%), in Southern Europe from 17 to 9.9 kt (42%) and in Northern Europe from 5.4 to 3.8 kt (29%) as compared to the same period in the last five years. BC emissions were slightly enhanced in Eastern Europe (from 28 to 31 kt) and remained unchanged in Scandinavia during the lockdown, due to increased residential

Deleted: of 11%

Deleted: Figure 9

Deleted: a

Deleted: of BC

Deleted: 20

Deleted: 23

Deleted: in France

Deleted: 44

Deleted: 39

Deleted: 11

Deleted: from 2.4

Deleted: 2.0

Deleted: from

Deleted: 2.2

Deleted: 1

Deleted: 3

Deleted: from

Deleted: 3.4

Deleted: 2

Deleted: 6

Deleted: 6.2

Deleted: 4.8

Deleted: 22

Deleted: 12

Deleted: 7.7

Deleted: 36

Deleted: 3.8

Deleted: 2

Deleted: 6

Deleted: 22

Deleted: 24

combustion, as people had to stay home and temperatures at that time were the lowest of the last five years. The presence of wood burning aerosols during the lockdowns was confirmed by large MERRA-2 AE, as well as from absorption AE measurements from AERONET that were higher in the lockdowns than in the same period of the last five years. The impact of the European lockdowns on BC emissions was also confirmed by a 11% decrease of the posterior emissions over Europe during the lockdowns, as compared to the period before, opposite to what was calculated in the previous years, which is obviously due to COVID-19. This decrease was more pronounced in France (42%), Italy (8%), Germany (21%), Spain (11%), UK (13%) and in Scandinavian countries (5%). The full impact of the disastrous pandemic will likely take years to assess. Nevertheless, with COVID-19 cases once again increasing in many countries, the information presented here are essential to understand the full health and climate impacts of lockdown measures.

Data availability. All measurement data and model outputs used for the present publication are open and can be downloaded from https://doi.org/10.21336/gen.b5vj-sn33 or upon request to the corresponding author. All prior emission datasets are also available for download. ECLIPSE emissions can be obtained from http://www.iiasa.ac.at/web/home/research/researchPrograms/air/Global_emissions.html, EDGAR version HTAP_V2.2 from http://edgar.jrc.ec.europa.eu/methodology.php#, ACCMIP version 5 from http://accent.aero.jussieu.fr/ACCMIP_metadata.php) and PKU from http://inventory.pku.edu.cn. FLEXPART is open in public and can be downloaded from https://www.flexpart.eu, so as FLEXINVERT+ from https://flexinvert.nilu.no. MERRA-2 re-analysis data can be obtained from https://disc.gsfc.nasa.gov, so as AERONET measurements from https://aeronet.gsfc.nasa.gov.

Author contributions. N.E. led the work and wrote the paper. S.E. and A.S. commented on the inversion framework. C.L.M., P.L., L.A.A., J.B., B.T.B., M.F., H.F., M.P., J.Y.D., N.P., J.P.P., K.S., M.S., K.E., S.V. and A.W. provided the ACTRIS measurements. S.M.P. gave recommendations on the MAC values used and wrote parts of the paper. All authors gave input in the writing process.

Competing interests. The authors declare no competing interests.

Acknowledgements. This study was supported by the Research Council of Norway (project ID: 275407, COMBAT – Quantification of Global Ammonia Sources constrained by a Bayesian Inversion Technique). N.E. and S.E. received funding from Arctic Monitoring & Assessment

Deleted: 10

Deleted: in the beginning of

Deleted: 0

Deleted: 11

Deleted: 32

Deleted: 5

Deleted: 25

Deleted: 12

Deleted: mac

Programme (AMAP). J.B. was supported by the Academy of Finland project Novel Assessment of Black Carbon in the Eurasian Arctic: From Historical Concentrations and Sources to Future Climate Impacts (NABCEA, project number 296302), and the Academy of Finland Centre of Excellence program (project number 307331) and COST Action CA16109 Chemical On-Line cOmpoSition and Source Apportionment of fine aerosoL, COLOSSAL. We thank B. Mougenot, O. Hagolle, A. Chaikovsky, P. Goloub, J. Lorente, R. Becker and M. Wiegner for their effort in establishing and maintaining the AERONET sites Ben Salem (Tunisia), Minsk (Belarus), Montsec (Spain), MetObs Lindenberg (Germany) and Munich University (Germany). The research leading to the ACTRIS measurements has received funding from the European Union's Horizon 2020 research and innovation programme under grant agreement No 654109 and the Cloudnet project (European Union contract EVK2-2000-00611).

References

Ackerman, a. S.: Reduction of Tropical Cloudiness by Soot, Science (80-.)., 288(5468), 1042–1047, doi:10.1126/science.288.5468.1042, 2000.

Adams, M. D.: Air pollution in Ontario, Canada during the COVID-19 State of Emergency, Sci. Total Environ., 742, 140516, doi:10.1016/j.scitotenv.2020.140516, 2020.

Bauwens, M., Compernolle, S., Stavrakou, T., Müller, J. F., van Gent, J., Eskes, H., Levelt, P. F., van der A, R., Veefkind, J. P., Vlietinck, J., Yu, H. and Zehner, C.: Impact of Coronavirus Outbreak on NO2 Pollution Assessed Using TROPOMI and OMI Observations, Geophys. Res. Lett., 47(11), 1–9, doi:10.1029/2020GL087978, 2020.

Bergamaschi, P., Krol, M., Meirink, J. F., Dentener, F., Segers, A., Van Aardenne, J., Monni, S., Vermeulen, A. T., Schmidt, M., Ramonet, M., Yver, C., Meinhardt, F., Nisbet, E. G., Fisher, R. E., O'Doherty, S. and Dlugokencky, E. J.: Inverse modeling of European CH4 emissions 2001-2006, J. Geophys. Res. Atmos., 115(22), 1–18, doi:10.1029/2010JD014180, 2010.

Berman, J. D. and Ebisu, K.: Changes in U.S. air pollution during the COVID-19 pandemic, Sci. Total Environ., 739, 139864, doi:10.1016/j.scitotenv.2020.139864, 2020.

Bond, T. C. and Bergstrom, R. W.: Light Absorption by Carbonaceous Particles: An Investigative Review, Aerosol Sci. Technol., 40(1), 27–67, doi:10.1080/02786820500421521, 2006.

Bond, T. C., Doherty, S. J., Fahey, D. W., Forster, P. M., Berntsen, T., Deangelo, B. J., Flanner, M. G., Ghan, S., Kärcher, B., Koch, D., Kinne, S., Kondo, Y., Quinn, P. K., Sarofim, M. C., Schultz, M. G., Schulz, M., Venkataraman, C., Zhang, H., Zhang, S., Bellouin, N., Guttikunda, S. K., Hopke, P. K., Jacobson, M. Z., Kaiser, J. W., Klimont, Z., Lohmann, U., Schwarz, J. P., Shindell, D., Storelvmo, T., Warren, S. G. and Zender, C. S.: Bounding the role of black carbon in the climate system: A scientific assessment, J. Geophys. Res. Atmos., 118(11), 5380–5552, doi:10.1002/jgrd.50171, 2013.

Buchard, V., Randles, C. A., da Silva, A. M., Darmenov, A., Colarco, P. R., Govindaraju, R., Ferrare, R., Hair, J., Beyersdorf, A. J., Ziemba, L. D. and Yu, H.: The MERRA-2 aerosol reanalysis, 1980 onward. Part II: Evaluation and case studies, J. Clim., 30(17), 6851–6872, doi:10.1175/JCLI-D-16-0613.1, 2017.

764 Cassiani, M., Stohl, A. and Brioude, J.: Lagrangian Stochastic Modelling of Dispersion in the
765 Convective Boundary Layer with Skewed Turbulence Conditions and a Vertical Density
766 Gradient: Formulation and Implementation in the FLEXPART Model, Boundary-Layer
767 Meteorol., 154(3), 367–390, doi:10.1007/s10546-014-9976-5, 2014.
768 Clarke, A. D. and Noone, K. J.: Soot in the arctic snowpack: a cause for perturbations in
769 radiative transfer, Atmos. Environ., 41(SUPPL.), 64–72, doi:10.1016/0004-6981(85)90113-1,
770 1985.
771 Conticini, E., Frediani, B. and Caro, D.: Can atmospheric pollution be considered a co-factor
772 in extremely high level of SARS-CoV-2 lethality in Northern Italy?, Environ. Pollut., 261,
773 114465, doi:10.1016/j.envpol.2020.114465, 2020.
774 Copernicus Climate Change Service (C3S): C3S ERA5-Land reanalysis . Copernicus Climate
775 Change Service, [online] Available from: https://cds.climate.copernicus.eu/cdsapp#!/home
776 (Accessed 31 August 2020), 2020.
777 Dantas, G., Siciliano, B., França, B. B., da Silva, C. M. and Arbilla, G.: The impact of
778 COVID-19 partial lockdown on the air quality of the city of Rio de Janeiro, Brazil, Sci. Total
779 Environ., 729, doi:10.1016/j.scitotenv.2020.139085, 2020.
780 Diffenbaugh, N. S., Field, C. B., Appel, E. A., Azevedo, I. L., Baldocchi, D. D., Burke, M.,
781 Burney, J. A., Ciais, P., Davis, S. J., Fiore, A. M., Fletcher, S. M., Hertel, T. W., Horton, D.
782 E., Hsiang, S. M., Jackson, R. B., Jin, X., Levi, M., Lobell, D. B., McKinley, G. A., Moore, F.
783 C., Montgomery, A., Nadeau, K. C., Pataki, D. E., Randerson, J. T., Reichstein, M., Schnell,
784 J. L., Seneviratne, S. I., Singh, D., Steiner, A. L. and Wong-Parodi, G.: The COVID-19
785 lockdowns: a window into the Earth System, Nat. Rev. Earth Environ., 1–12,
786 doi:10.1038/s43017-020-0079-1, 2020.
787 Dutheil, F., Baker, J. S. and Navel, V.: COVID-19 as a factor influencing air pollution?,
788 Environ. Pollut., 263, 2019–2021, doi:10.1016/j.envpol.2020.114466, 2020.
789 Eck, T. F., Holben, B. N., Reid, J. S., Smirnov, A., Neill, N. T. O., Slutsker, I. and Kinne, S.:
790 Wavelength dependence of the optical depth of biomass burning, urban, and desert dust
791 aerosols, J. Geophys. Res., 104(D24), 31333–31349, 1999.
792 Evangeliou, N., Thompson, R. L., Eckhardt, S. and Stohl, A.: Top-down estimates of black
793 carbon emissions at high latitudes using an atmospheric transport model and a Bayesian
794 inversion framework, Atmos. Chem. Phys., 18(20), doi:10.5194/acp-18-15307-2018, 2018.
795 Forster, C., Stohl, A. and Seibert, P.: Parameterization of convective transport in a Lagrangian
796 particle dispersion model and its evaluation, J. Appl. Meteorol. Climatol., 46(4), 403–422,
797 doi:10.1175/JAM2470.1, 2007.
798 Giglio, L., Descloitres, J., Justice, C. O. and Kaufman, Y. J.: An enhanced contextual fire
799 detection algorithm for MODIS, Remote Sens. Environ., 87(2–3), 273–282,
800 doi:10.1016/S0034-4257(03)00184-6, 2003.
801 Giglio, L., Randerson, J. T. and van der Werf, G. R.: Analysis of daily, monthly, and annual
802 burned area using the fourth-generation global fire emissions database (GFED4), J. Geophys.
803 Res. Biogeosciences, 118, 317–328, doi:10.1002/jgrg.20042, 2013, 2013.
804 Grythe, H., Kristiansen, N. I., Groot Zwaaftink, C. D., Eckhardt, S., Ström, J., Tunved, P.,
805 Krejci, R. and Stohl, A.: A new aerosol wet removal scheme for the Lagrangian particle
806 model FLEXPARTv10, Geosci. Model Dev., 10, 1447–1466, doi:10.5194/gmd-10-1447-
807 2017, 2017.
808 Gueymard, C. A. and Yang, D.: Worldwide validation of CAMS and MERRA-2 reanalysis
809 aerosol optical depth products using 15 years of AERONET observations, Atmos. Environ.,
810 225(November 2019), 117216, doi:10.1016/j.atmosenv.2019.117216, 2020.
811 He, G., Pan, Y. and Tanaka, T.: The short-term impacts of COVID-19 lockdown on urban air
812 pollution in China, Nat. Sustain., doi:10.1038/s41893-020-0581-y, 2020.
813 Hegg, D. A., Warren, S. G., Grenfell, T. C., Doherty, S. J., Larson, T. V. and Clarke, A. D.:

814 Source attribution of black carbon in arctic snow, Environ. Sci. Technol., 43(11), 4016–4021,
815 doi:10.1021/es803623f, 2009.
816 Holben, B. N., Eck, T. F., Slutsker, I., Tanré, D., Buis, J. P., Setzer, A., Vermote, E., Reagan,
817 J. A., Kaufman, Y. J., Nakajima, T., Lavenu, F., Jankowiak, I. and Smirnov, A.:
818 AERONET—A Federated Instrument Network and Data Archive for Aerosol
819 Characterization, Remote Sens. Environ., 66(1), 1–16, doi:10.1016/S0034-4257(98)00031-5,
820 1998.
821 Huang, C., Wang, Y., Li, X., Ren, L., Zhao, J., Hu, Y., Zhang, L., Fan, G., Xu, J., Gu, X.,
822 Cheng, Z., Yu, T., Xia, J., Wei, Y., Wu, W., Xie, X., Yin, W., Li, H., Liu, M., Xiao, Y., Gao,
823 H., Guo, L., Xie, J., Wang, G., Jiang, R., Gao, Z., Jin, Q., Wang, J. and Cao, B.: Clinical
824 features of patients infected with 2019 novel coronavirus in Wuhan, China, Lancet,
825 395(10223), 497–506, doi:10.1016/S0140-6736(20)30183-5, 2020.
826 Janssens-Maenhout, G., Crippa, M., Guizzardi, D., Dentener, F., Muntean, M., Pouliot, G.,
827 Keating, T., Zhang, Q., Kurokawa, J., Wankmüller, R., Denier Van Der Gon, H., Kuenen, J. J.
828 P., Klimont, Z., Frost, G., Darras, S., Koffi, B. and Li, M.: HTAP-v2.2: A mosaic of regional
829 and global emission grid maps for 2008 and 2010 to study hemispheric transport of air
830 pollution, Atmos. Chem. Phys., 15(19), 11411–11432, doi:10.5194/acp-15-11411-2015, 2015.
831 Jinhuan, Q. and Liquan, Y.: Variation characteristics of atmospheric aerosol optical depths
832 and visibility in North China during 1980 } 1994, Atmos. Environ., 34, 603–609, 2000.
833 John Hopkins University of Medicine: Coronavirus resource center, [online] Available from:
834 https://coronavirus.jhu.edu/map.html (Accessed 10 August 2020), 2020.
835 Kaminski, T., Rayner, P. J., Heimann, M. and Enting, I. G.: On aggregation errors in
836 atmospheric transport inversions, J. Geophys. Res. Atmos., 106(D5), 4703–4715,
837 doi:10.1029/2000JD900581, 2001.
838 Kerimray, A., Baimatova, N., Ibragimova, O. P., Bukenov, B., Kenessov, B., Plotitsyn, P. and
839 Karaca, F.: Assessing air quality changes in large cities during COVID-19 lockdowns: The
840 impacts of traffic-free urban conditions in Almaty, Kazakhstan, Sci. Total Environ., 730,
841 139179, doi:10.1016/j.scitotenv.2020.139179, 2020.
842 Klimont, Z., Kupiainen, K., Heyes, C., Purohit, P., Cofala, J., Rafaj, P., Borken-Kleefeld, J.
843 and Schöpp, W.: Global anthropogenic emissions of particulate matter including black
844 carbon, Atmos. Chem. Phys., 17, 8681–8723, doi:10.5194/acp-17- 50 8681-2017, 2017.
845 Kummu, M., Taka, M. and Guillaume, J. H. A.: Data from: Gridded global datasets for Gross
846 Domestic Product and Human Development Index over 1990-2015, v2, Dryad, Dataset,
847 doi:https://doi.org/10.5061/dryad.dk1j0, 2020.
848 Lack, D. A. and Langridge, J. M.: On the attribution of black and brown carbon light
849 absorption using the Ångström exponent, Atmos. Chem. Phys., 13(20), 10535–10543,
850 doi:10.5194/acp-13-10535-2013, 2013.
851 Laj, P., Bigi, A., Rose, C., Andrews, E., Lund Myhre, C., Collaud Coen, M., Wiedensohler,
852 A., Schultz, M., Ogren, J., Fiebig, M., Gliß, J., Mortier, A., Pandolfi, M., Petäjä, T., Kim, S.-
853 W., Aas, W., Putaud, J.-P., Mayol-Bracero, O., Keywood, M., Labrador, L., Aalto, P.,
854 Ahlberg, E., Alados Arboledas, L., Alastuey, A., Andrade, M., Artíñano, B., Ausmeel, S.,
855 Arsov, T., Asmi, E., Backman, J., Baltensperger, U., Bastian, S., Bath, O., Beukes, J. P.,
856 Brem, B., Bukowiecki, N., Conil, S., Couret, C., Day, D., Dayantolis, W., Degorska, A., Dos
857 Santos, S. M., Eleftheriadis, K., Fetfatzis, P., Favez, O., Flentje, H., Gini, M., Gregorič, A.,
858 Gysel-Beer, M., Hallar, G., Hand, J., Hoffer, A., Hueglin, C., Hooda, R., Hyvärinen, A.,
859 Kalapov, I., Kalivitis, N., Kasper-Giebl, A., Kim, J. E., Kouvarakis, G., Kranjc, I., Krejci, R.,
860 Kulmala, M., Labuschagne, C., Lee, H.-J., Lihavainen, H., Lin, N.-H., Löschau, G., Luoma,
861 K., Marinoni, A., Meinhardt, F., Merkel, M., Metzger, J.-M., Mihalopoulos, N., Nguyen, N.
862 A., Ondracek, J., Peréz, N., Perrone, M. R., Petit, J.-E., Picard, D., Pichon, J.-M., Pont, V.,
863 Prats, N., Prenni, A., Reisen, F., Romano, S., Sellegri, K., Sharma, S., Schauer, G., Sheridan,

P., Sherman, J. P., Schütze, M., Schwerin, A., Sohmer, R., Sorribas, M., Steinbacher, M., Sun, J., Titos, G., Tokzko, B., et al.: A global analysis of climate-relevant aerosol properties retrieved from the network of GAW near-surface observatories, Atmos. Meas. Tech. Discuss., 1–70, doi:10.5194/amt-2019-499, 2020.
Lamarque, J. F., Shindell, D. T., Josse, B., Young, P. J., Cionni, I., Eyring, V., Bergmann, D., Cameron-Smith, P., Collins, W. J., Doherty, R., Dalsoren, S., Faluvegi, G., Folberth, G., Ghan, S. J., Horowitz, L. W., Lee, Y. H., MacKenzie, I. A., Nagashima, T., Naik, V., Plummer, D., Righi, M., Rumbold, S. T., Schulz, M., Skeie, R. B., Stevenson, D. S., Strode, S., Sudo, K., Szopa, S., Voulgarakis, A. and Zeng, G.: The atmospheric chemistry and climate model intercomparison Project (ACCMIP): Overview and description of models, simulations and climate diagnostics, Geosci. Model Dev., 6(1), 179–206, doi:10.5194/gmd-6-179-2013, 2013.
Le, T., Wang, Y., Liu, L., Yang, J., Yung, Y. L., Li, G. and Seinfeld, J. H.: Unexpected air pollution with marked emission reductions during the COVID-19 outbreak in China, Science (80-.)., (2), eabb7431, doi:10.1126/science.abb7431, 2020.
Lian, X., Huang, J., Huang, R., Liu, C., Wang, L. and Zhang, T.: Impact of city lockdown on the air quality of COVID-19-hit of Wuhan city, Sci. Total Environ., 742, 140556, doi:10.1016/j.scitotenv.2020.140556, 2020.
Long, C. M., Nascarella, M. A. and Valberg, P. A.: Carbon black vs. black carbon and other airborne materials containing elemental carbon: Physical and chemical distinctions, Environ. Pollut., 181, 271–286, doi:10.1016/j.envpol.2013.06.009, 2013.
Myhre, G., Samset, B. H., Schulz, M., Balkanski, Y., Bauer, S., Berntsen, T. K., Bian, H., Bellouin, N., Chin, M., Diehl, T., Easter, R. C., Feichter, J., Ghan, S. J., Hauglustaine, D., Iversen, T., Kinne, S., Kirkeväg, A., Lamarque, J. F., Lin, G., Liu, X., Lund, M. T., Luo, G., Ma, X., Van Noije, T., Penner, J. E., Rasch, P. J., Ruiz, A., Seland, Skeie, R. B., Stier, P., Takemura, T., Tsigaridis, K., Wang, P., Wang, Z., Xu, L., Yu, H., Yu, F., Yoon, J. H., Zhang, K., Zhang, H. and Zhou, C.: Radiative forcing of the direct aerosol effect from AeroCom Phase II simulations, Atmos. Chem. Phys., 13(4), 1853–1877, doi:10.5194/acp-13-1853-2013, 2013.
Otmani, A., Benchrif, A., Tahri, M., Bounakhla, M., Chakir, E. M., El Bouch, M. and Krombi, M.: Impact of Covid-19 lockdown on PM10, SO2 and NO2 concentrations in Salé City (Morocco), Sci. Total Environ., 735(2), 139541, doi:10.1016/j.scitotenv.2020.139541, 2020.
Petzold, A., Ogren, J. A., Fiebig, M., Laj, P., Li, S. M., Baltensperger, U., Holzer-Popp, T., Kinne, S., Pappalardo, G., Sugimoto, N., Wehrli, C., Wiedensohler, A. and Zhang, X. Y.: Recommendations for reporting black carbon measurements, Atmos. Chem. Phys., 13(16), 8365–8379, doi:10.5194/acp-13-8365-2013, 2013.
Pisso, I., Sollum, E., Grythe, H., Kristiansen, N., Cassiani, M., Eckhardt, S., Arnold, D., Morton, D., Thompson, R. L., Groot Zwaaftink, C. D., Evangeliou, N., Sodemann, H., Haimberger, L., Henne, S., Brunner, D., Burkhart, J. F., Fouilloux, A., Brioude, J., Philipp, A., Seibert, P. and Stohl, A.: The Lagrangian particle dispersion model FLEXPART version 10.4, Geosci. Model Dev., 12, 4955–4997, doi:10.5194/gmd-12-4955-2019, 2019.
Qin, W., Zhang, Y., Chen, J., Yu, Q., Cheng, S., Li, W., Liu, X. and Tian, H.: Variation, sources and historical trend of black carbon in Beijing, China based on ground observation and MERRA-2 reanalysis data, Environ. Pollut., 245(2), 853–863, doi:10.1016/j.envpol.2018.11.063, 2019.
Quayle, R. G. and Diaz, H. F.: Heating degree day data applied to residential heating energy consumption, J. Appl. Meteorol., 19, 241–246, 1980.
Le Quéré, C., Jackson, R. B., Jones, M. W., Smith, A. J. P., Abernethy, S., Andrew, R. M., De-Gol, A. J., Willis, D. R., Shan, Y., Canadell, J. G., Friedlingstein, P., Creutzig, F. and

914 Peters, G. P.: Temporary reduction in daily global CO2 emissions during the COVID-19
915 forced confinement, Nat. Clim. Chang., 10(7), 647–653, doi:10.1038/s41558-020-0797-x,
916 2020.
917 Randles, C. A., da Silva, A. M., Buchard, V., Colarco, P. R., Darmenov, A., Govindaraju, R.,
918 Smirnov, A., Holben, B., Ferrare, R., Hair, J., Shinozuka, Y. and Flynn, C. J.: The MERRA-2
919 aerosol reanalysis, 1980 onward. Part I: System description and data assimilation evaluation,
920 J. Clim., 30(17), 6823–6850, doi:10.1175/JCLI-D-16-0609.1, 2017.
921 Sicard, P., De Marco, A., Agathokleous, E., Feng, Z., Xu, X., Paoletti, E., Rodriguez, J. J. D.
922 and Calatayud, V.: Amplified ozone pollution in cities during the COVID-19 lockdown, Sci.
923 Total Environ., 735, doi:10.1016/j.scitotenv.2020.139542, 2020.
924 Sohrabi, C., Alsafi, Z., O'Neill, N., Khan, M., Kerwan, A., Al-Jabir, A., Iosifidis, C. and
925 Agha, R.: World Health Organization declares global emergency: A review of the 2019 novel
926 coronavirus (COVID-19), Int. J. Surg., 76(February), 71–76, doi:10.1016/j.ijsu.2020.02.034,
927 2020.
928 Stohl, A., Forster, C., Frank, A., Seibert, P. and Wotawa, G.: Technical note: The Lagrangian
929 particle dispersion model FLEXPART version 6.2, Atmos. Chem. Phys., 5(9), 2461–2474,
930 doi:10.5194/acp-5-2461-2005, 2005.
931 Stohl, A., Kim, J., Li, S., O'Doherty, S., Salameh, P. K., Saito, T., Vollmer, M. K., Wan, D.,
932 Yao, B., Yokouchi, Y. and Zhou, L. X.: Hydrochlorofluorocarbon and hydrofluorocarbon
933 emissions in East Asia determined by inverse modeling, Atmos. Chem. Phys. Discuss., 10(2),
934 2089–2129, doi:10.5194/acpd-10-2089-2010, 2010.
935 Stohl, A., Klimont, Z., Eckhardt, S., Kupiainen, K., Shevchenko, V. P., Kopeikin, V. M. and
936 Novigatsky, A. N.: Black carbon in the Arctic: The underestimated role of gas flaring and
937 residential combustion emissions, Atmos. Chem. Phys., 13(17), 8833–8855, doi:10.5194/acp-
938 13-8833-2013, 2013.
939 Sun, E., Xu, X., Che, H., Tang, Z., Gui, K., An, L., Lu, C. and Shi, G.: Variation in MERRA-
940 2 aerosol optical depth and absorption aerosol optical depth over China from 1980 to 2017, J.
941 Atmos. Solar-Terrestrial Phys., 186(January), 8–19, doi:10.1016/j.jastp.2019.01.019, 2019.
942 Tarantola, A.: Inverse Problem Theory and Methods for Model Parameter Estimation, Society
943 for Industrial and Applied Mathematics, Philadelphia, Pa., 2005.
944 Thacker, W. C.: Data assimilation with inequality constraints, Ocean Model., 16(3–4), 264–
945 276, doi:10.1016/j.ocemod.2006.11.001, 2007.
946 Thompson, R. L. and Stohl, A.: FLEXINVERT: An atmospheric Bayesian inversion
947 framework for determining surface fluxes of trace species using an optimized grid, Geosci.
948 Model Dev., 7(5), 2223–2242, doi:10.5194/gmd-7-2223-2014, 2014.
949 Thompson, R. L., Stohl, A., Zhou, L. X., Dlugokencky, E., Fukuyama, Y., Tohjima, Y., Kim,
950 S. Y., Lee, H., Nisbet, E. G., Fisher, R. E., Lowry, D., Weiss, R. F., Prinn, R. G., O'Doherty,
951 S., Young, D. and White, J. W. C.: Methane emissions in East Asia for 2000-2011 estimated
952 using an atmospheric Bayesian inversion, J. Geophys. Res. Atmos., 120(9), 4352–4369,
953 doi:10.1002/2014JD022394, 2015.
954 Wang, P., Wang, H., Wang, Y. Q., Zhang, X. Y., Gong, S. L., Xue, M., Zhou, C. H., Liu, H.
955 L., An, X. Q., Niu, T. and Cheng, Y. L.: Inverse modeling of black carbon emissions over
956 China using ensemble data assimilation, Atmos. Chem. Phys., 16(2), 989–1002,
957 doi:10.5194/acp-16-989-2016, 2016.
958 Wang, R., Tao, S., Balkanski, Y., Ciais, P., Boucher, O., Liu, J., Piao, S., Shen, H., Vuolo, M.
959 R., Valari, M., Chen, H., Chen, Y., Cozic, A., Huang, Y., Li, B., Li, W., Shen, G., Wang, B.
960 and Zhang, Y.: Exposure to ambient black carbon derived from a unique inventory and high-
961 resolution model., Proc. Natl. Acad. Sci. U. S. A., 111(7), 2459–63,
962 doi:10.1073/pnas.1318763111, 2014a.
963 Wang, R., Tao, S., Shen, H., Huang, Y., Chen, H., Balkanski, Y., Boucher, O., Ciais, P.,

964 Shen, G., Li, W., Zhang, Y., Chen, Y., Lin, N., Su, S., Li, B., Liu, J. and Liu, W.: Trend in
965 global black carbon emissions from 1960 to 2007, Environ. Sci. Technol., 48(12), 6780–6787,
966 doi:10.1021/es5021422, 2014b.
967 WHO: Report of the WHO-China Joint Mission on Coronavirus Disease 2019 (COVID-19),
968 WHO-China Jt. Mission Coronavirus Dis. 2019, 2019(February), 16–24 [online] Available
969 from: https://www.who.int/docs/default-source/coronaviruse/who-china-joint-mission-on-
970 covid-19-final-report.pdf, 2020.
971 Zanatta, M., Gysel, M., Bukowiecki, N., M??ller, T., Weingartner, E., Areskoug, H., Fiebig,
972 M., Yttri, K. E., Mihalopoulos, N., Kouvarakis, G., Beddows, D., Harrison, R. M., Cavalli, F.,
973 Putaud, J. P., Spindler, G., Wiedensohler, A., Alastuey, A., Pandolfi, M., Sellegri, K.,
974 Swietlicki, E., Jaffrezo, J. L., Baltensperger, U. and Laj, P.: A European aerosol
975 phenomenology-5: Climatology of black carbon optical properties at 9 regional background
976 sites across Europe, Atmos. Environ., 145, 346–364, doi:10.1016/j.atmosenv.2016.09.035,
977 2016.
978 Zheng, H., Kong, S., Chen, N., Yan, Y., Liu, D., Zhu, B., Xu, K., Cao, W., Ding, Q., Lan, B.,
979 Zhang, Z., Zheng, M., Fan, Z., Cheng, Y., Zheng, S., Yao, L., Bai, Y., Zhao, T. and Qi, S.:
980 Significant changes in the chemical compositions and sources of PM2.5 in Wuhan since the
981 city lockdown as COVID-19, Sci. Total Environ., 739, doi:10.1016/j.scitotenv.2020.140000,
982 2020.
983 Zotter, P., Herich, H., Gysel, M., El-Haddad, I., Zhang, Y., Mocnik, G., Hüglin, C.,
984 Baltensperger, U., Szidat, S. and Prévôt, A. S. H.: Evaluation of the absorption Ångström
985 exponents for traffic and wood burning in the Aethalometer-based source apportionment
986 using radiocarbon measurements of ambient aerosol, Atmos. Chem. Phys., 17(6), 4229–4249,
987 doi:10.5194/acp-17-4229-2017, 2017.
988
989

990 **TABLES & FIGURES**

991

992 **Table 1.** Observation sites from the ACTRIS platform used to perform the inversions
993 (dependent observations) and to validate the posterior emissions (independent observations)
994 (the altitude indicates the sampling height in meters above sea level). Multi-Angle Absorption
995 Photometers (MAAP) were used at all sites, except El Arenosillo (ES0100R) where a
996 Continuous Light Absorption Photometer (CLAP) was used, Birkenes (NO0002R), where a
997 Particle Soot Absorption Photometer (PSAP) and Observatoire Perenne de l' Environnement
998 (FR0022R) and Zeppelin (NO0042G) where Aethalometers (AW31) were used.

Name	Latitude	Longitude	Altitude	Type	Wavelength (nm)	$MAC_{@637}$ (m^2 g^{-1})
Jungfraujoch (CH0001G)	46.55	7.99	3578	Dependent	637	10
Hohenpeissenberg (DE0043G)	47.80	11.01	985	Dependent	660	9.65
Melpitz (DE0044K)	51.53	12.93	86	Dependent	670	8.78
Zugspitze-Schneefernerhaus (DE0054R)	47.42	10.98	2671	Independent	670	9.51
Leipzig-Eisenbahnstrasse (DE0066K)	51.35	12.41	120	Independent	670	9.51
Izaña (ES0018G)	28.41	-16.50	2373	Dependent	670	9.51
Granada (ES0020U)	37.16	-3.61	680	Dependent	670	9.51
Montsec (ES0022R)	42.05	0.73	1571	Dependent	670	9.51
El Arenosillo (ES0100R)	37.10	-6.73	41	Dependent	652	13.64
Montseny (ES1778R)	41.77	2.35	700	Dependent	670	8.48
Pallas (FI0096G)	67.97	24.12	565	Dependent	637	10.00
Observatoire Perenne de l' Environnement (FR0022R)	48.56	5.51	392	Dependent	880	7.24
Puy de Dôme (FR0030R)	45.77	2.96	1465	Dependent	670	9.51
Ispra (IT0004R)	45.80	8.63	209	Dependent	880	6.96
Mt Cimone (IT0009R)	44.18	10.70	2165	Dependent	670	9.51
Birkenes II (NO0002R)	58.39	8.25	219	Dependent	660	7.59
Zeppelin mountain (NO0042G)	78.91	11.89	474	Dependent	880	7.24

999

Table 2. Statistical measures (***RMSE***, Pearson's R^2, ***MFB*** and ***nMAE***) for each of the prior and posterior concentrations against dependent observations (observations that were used in the inversion algorithm) for BC (eBC). Note that the inversion using ECLIPSEv6 prior emission dataset gave the best agreement with the observations and therefore the results of this inversion are presented here.

	nRMSE	**Pearson's R^2**	**MFB**	**nMAE**
Prior ECLIPSEv6	0.102	0.30	0.52	997
Prior ECLIPSEv5	0.098	0.18	-0.04	996
Prior EDGAR_HTAPv2.2	0.105	0.11	0.34	1017
Prior ACCMIPv5	0.101	0.28	0.36	971
Prior PKU	0.101	0.21	0.25	983
Posterior ECLIPSEv6	**0.073**	**0.60**	**0.03**	**714**
Posterior ECLIPSEv5	0.084	0.52	0.09	819
Posterior EDGAR_HTAPv2.2	0.084	0.53	0.20	815
Posterior ACCMIPv5	0.091	0.55	0.26	787
Posterior PKU	0.082	0.55	0.24	795

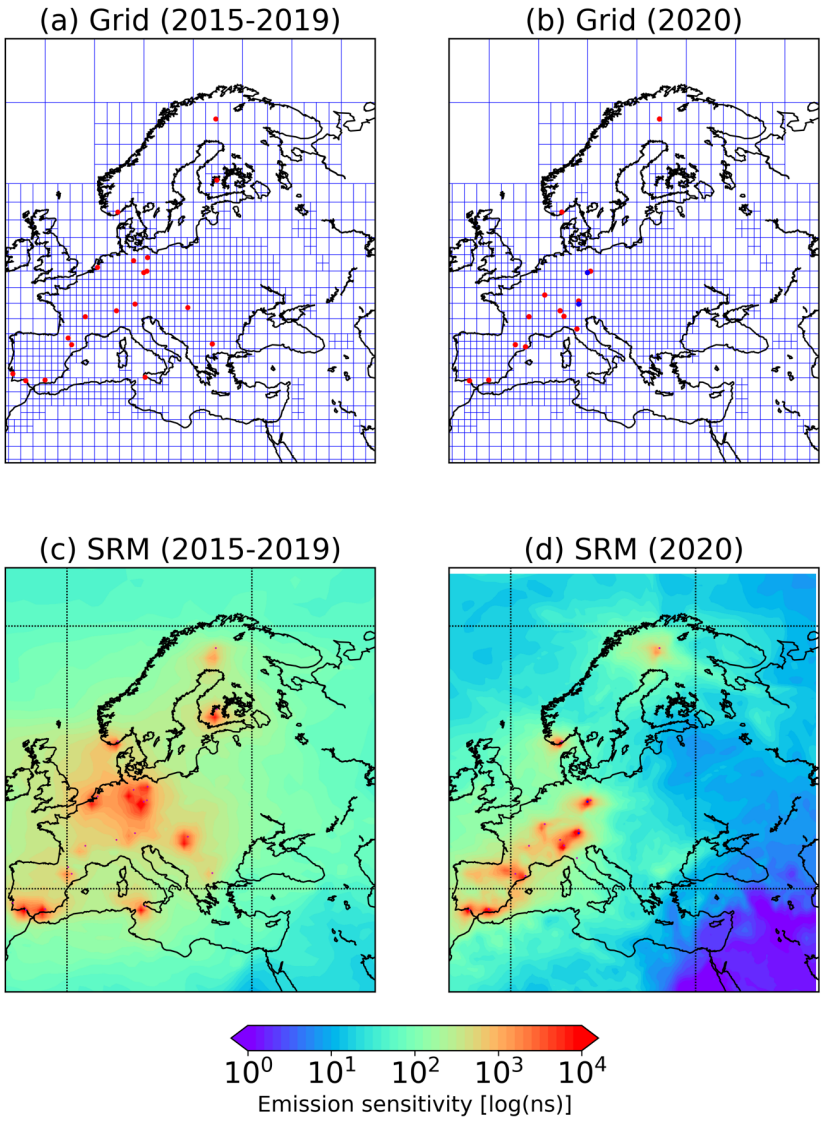

Figure 1. Aggregated inversion grid used for the (a) 2015–2019 and (b) 2020 inversions, respectively. The dependent measurements that were used in the inversion were taken from stations highlighted in red. The two independent stations that were used for the validation are shown in blue. (c, d) Footprint emission sensitivity (i.e. SRM) averaged over all observations and time steps for each of the inversions. Red points denote the location of each measurement site.

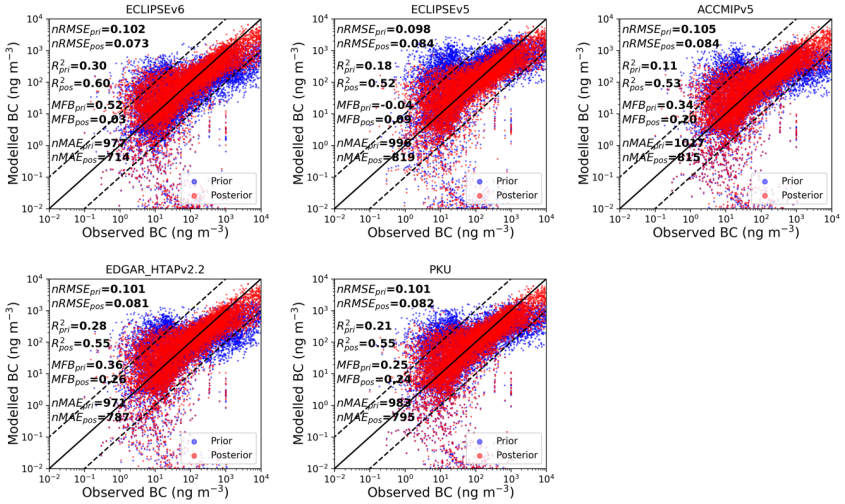

Figure 2. Scatter plots of prior and posterior concentrations against dependent observations (observations that were included in the inversion framework) from ACTRIS from January to April 2020. Four statistical measures (***nRMSE***, Pearson's $\boldsymbol{R^2}$, ***MFB*** and ***nMAE***) were used to assess the performance of each inversion using five different prior emission inventories for BC (ECLIPSEv5, v6, ACCMIPv5, EDGAR_HTAPv2.2 and PKU).

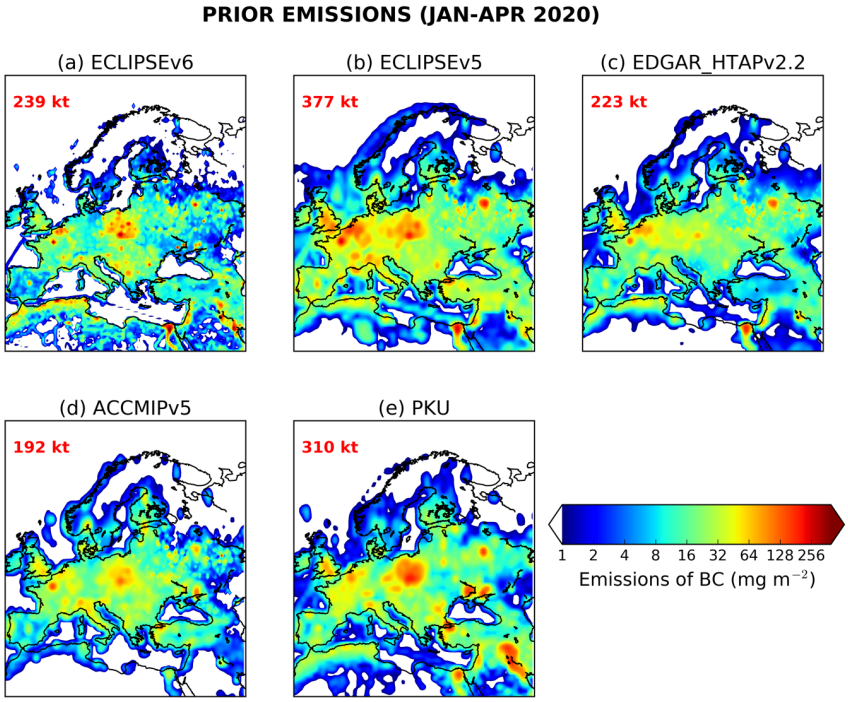

Figure 3. Prior emissions of black carbon (BC) used in the inversions. BC emissions from anthropogenic sources were adopted from ECLIPSE version 5 and 6 (Evaluating the CLimate and Air Quality ImPacts of ShortlivEd Pollutants) (Klimont et al., 2017), EDGAR (Emissions Database for Global Atmospheric Research) version HTAP_v2.2 (Janssens-Maenhout et al., 2015), ACCMIP (Emissions for Atmospheric Chemistry and Climate Model Intercomparison Project) version 5 (Lamarque et al., 2013) and PKU (Peking University) (Wang et al., 2014b). Biomass burning emissions of BC from Global Fire Emissions Database (GFED) version 4.1 (Giglio et al., 2013) were added in each of the aforementioned inventories.

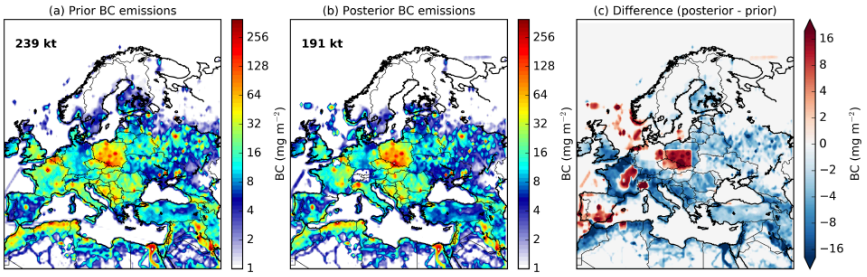

Figure 4. (a) Prior emissions of BC from ECLIPSEv6, (b) optimized (posterior) BC emissions after processing the ACTRIS data into the inversion algorithm, and (c) difference between posterior and prior emissions. All the results correspond to the inversion yielding the best results (Table 2 and Figure 2).

Deleted:

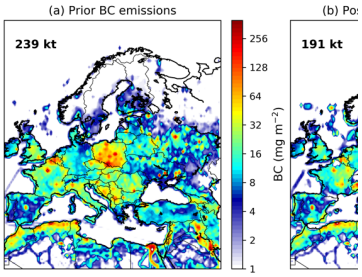

Deleted: Table 2

Deleted: Figure 2

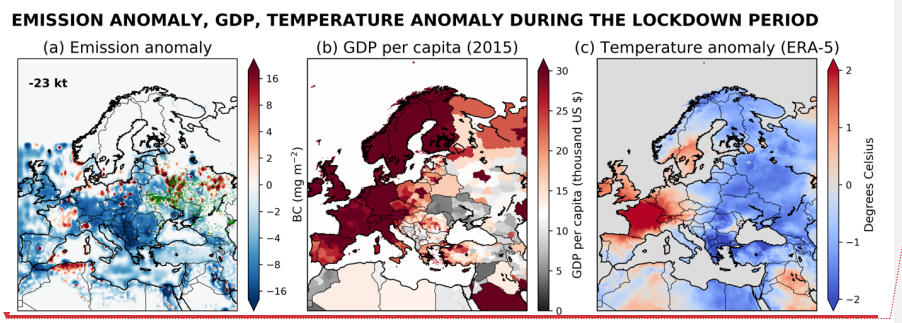

Figure 5. (a) Difference in posterior BC emissions during the lockdown (14 March to 30 April 2020) in Europe from the respective emissions during the same period in 2015 – 2019, (b) GDP from Kummu et al. (2020), and (c) temperature anomaly from ERA-5 (Copernicus Climate Change Service (C3S), 2020) for the same period as the emission anomaly. The base GDP value below which a low income can be assumed was set to 12 thousand US dollars. Active fires from MODIS are plotted together with emission anomaly (green dots).

Deleted:

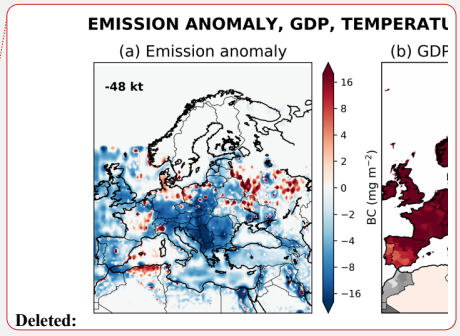

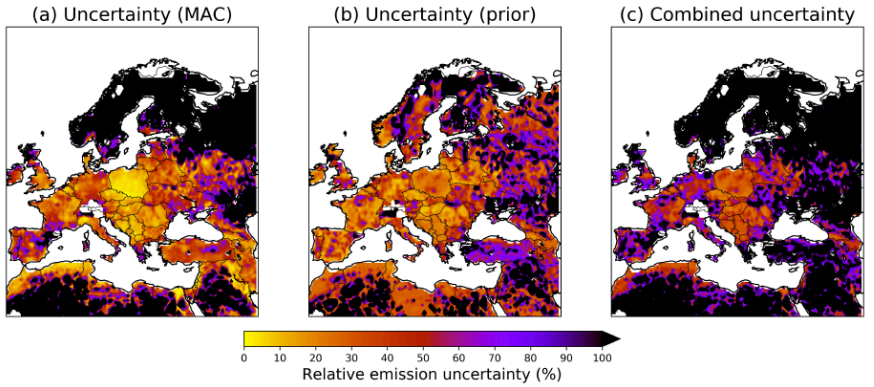

Figure 6. (a) Uncertainty of BC emissions due to the use of variable MAC values to convert from aerosol absorption to eBC concentrations that are used by the inversion algorithm. (b) Uncertainty due to the use of five different prior emissions inventories for BC. (c) Combined uncertainty.

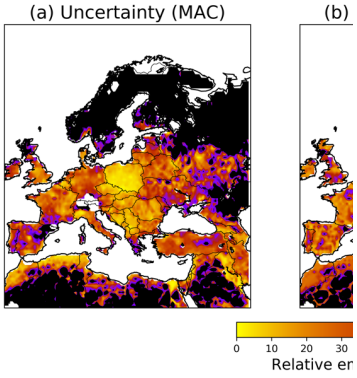

Deleted:

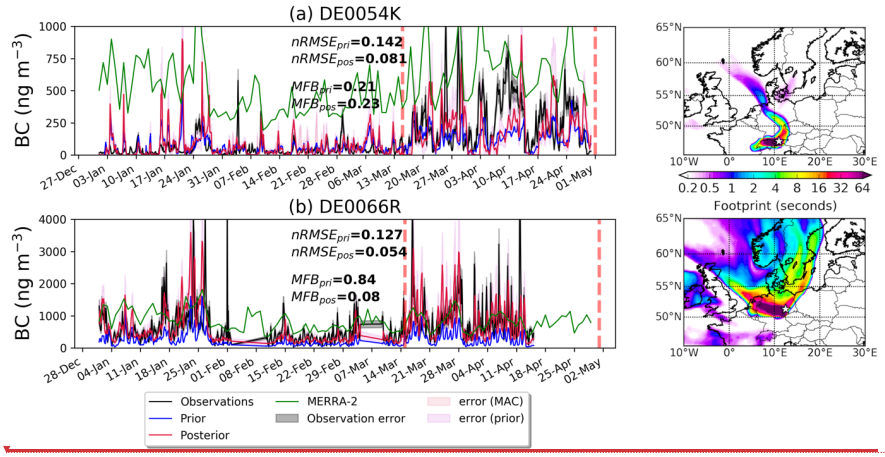

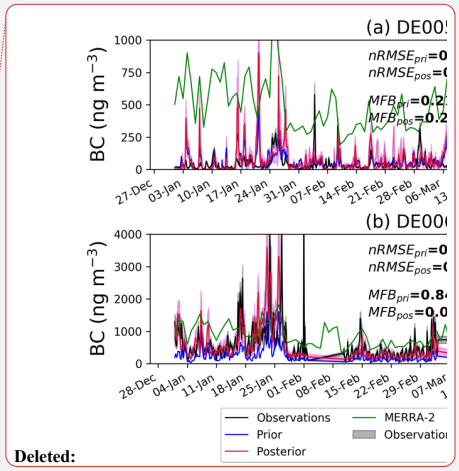

Deleted:

Figure 7. Prior and posterior BC concentrations at DE0054K and DE0066R stations that were not included in the inversion are compared with observations. The validation is done by calculating the ***nRMSEs*** and ***MFBs*** for the prior and posterior concentrations. The uncertainty of the observations is also given together with the posterior uncertainties in the concentrations calculated from the use of different MAC and prior emissions. For comparison, we plot the concentrations from MERRA-2 at the same two stations. The vertical dashed lines denote the period of the lockdown in most of Europe. On the right, the average footprint emission sensitivities are given at each independent station for the period of the lockdown.

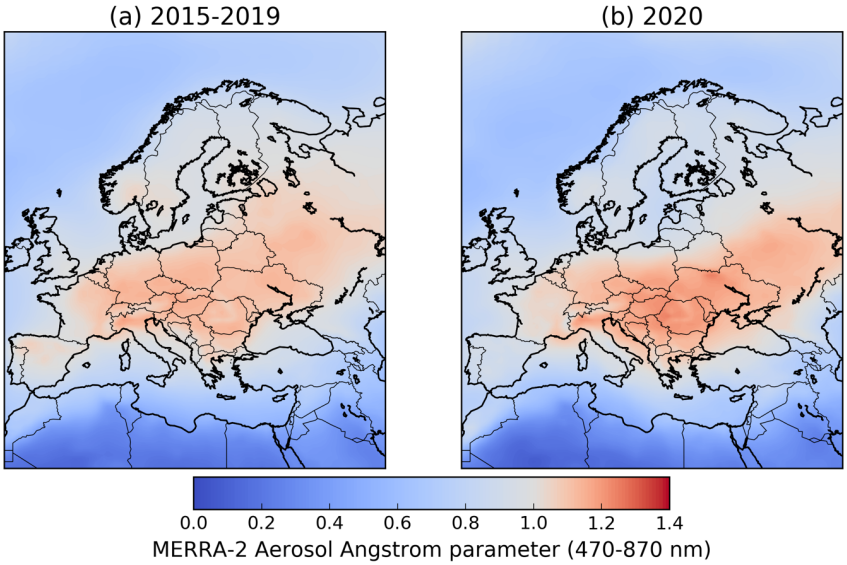

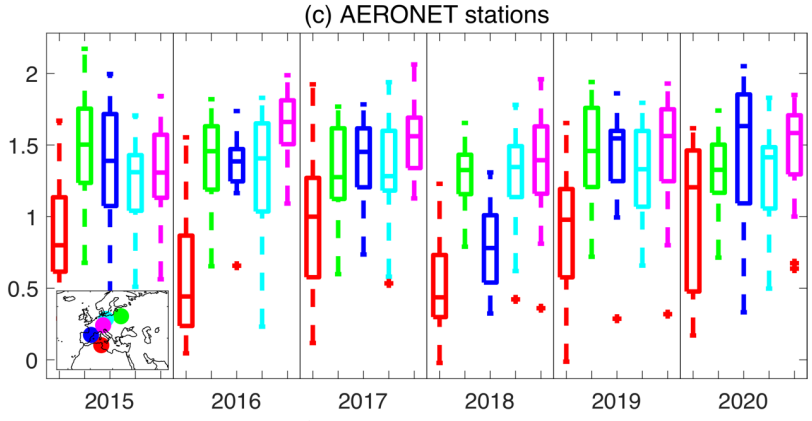

Figure 8. (a) Average total aerosol Ångström parameter (470-870 nm) over Europe (mid-March to April) in the five previous years (2015–2019) and (b) in 2020 (lockdown). (c) AERONET Absorption AE in Ben Salem (9.91°E, 35.55°N, in red), Minsk (27.60°E, 53.92°N, green), Montsec (0.73°E, 42.05°N, blue), MetObs Lindenberg (14.12°E, 52.21°N, magenta) and Munich University (11.57°E, 48.15°N) during mid-March to April in all years since 2015.

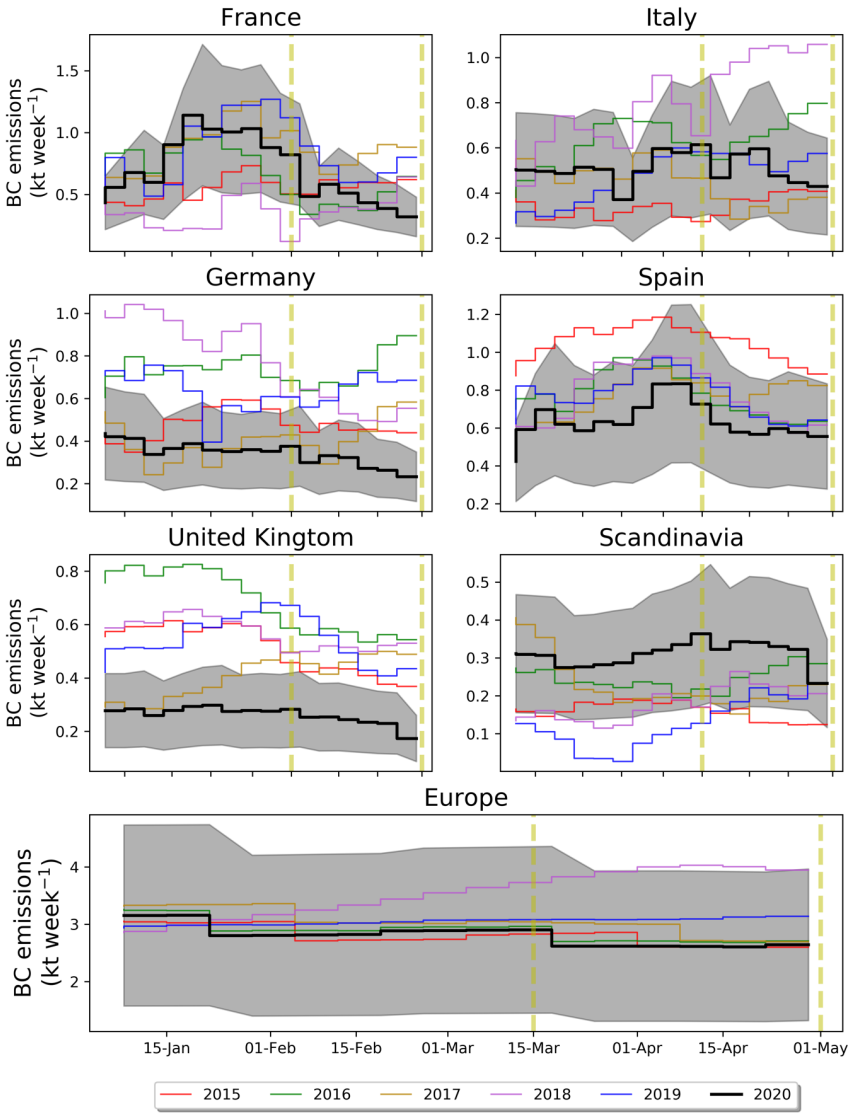

Figure 9. Posterior BC emissions in the most highly affected European countries (France, Italy, Germany, Spain and UK), Scandinavia and Europe from the COVID-19 pandemic (2020). Posterior BC emissions for every year since 2015 are also plotted in the same temporal resolution to show changes in BC emissions characteristics during the 2020 COVID-19 pandemic. The grey shaded area corresponds to the BC emission uncertainty, while the vertical yellow dashed lines correspond to the beginning and end of the 2020 lockdown.